[redacted]

Technical Report No. 37

SACLANT ASW
RESEARCH CENTRE

EM PHENOMENA IN THE ELF RANGE: NATURAL BACKGROUND NOISE AND INSTRUMENTATION FOR ITS MEASUREMENT

by

L. BROCK-NANNESTAD

15 JUNE 1965

[redacted]

VIALE SAN BARTOLOMEO, 92
LA SPEZIA, ITALY

[redacted]

TECHNICAL REPORT NO. 37

SACLANT ASW RESEARCH CENTRE
Viale San Bartolomeo 92
La Spezia, Italy

EM PHENOMENA IN THE ELF RANGE:

NATURAL BACKGROUND NOISE AND INSTRUMENTATION FOR ITS MEASUREMENT

By

L. Brock-Nannestad

15 June 1965

APPROVED FOR DISTRIBUTION

HENRIK NØDTVEDT
Director

TABLE OF CONTENTS

TABLE OF CONTENTS (Continued)

Page

FIGURES

EM PHENOMENA IN THE ELF RANGE

By

L. Brock-Nannestad

PREFACE TO THE SERIES

The series of three reports published under the general heading of "Electromagnetic Phenomena in the Extremely Low Frequency Range" provides a final summary of the research in this field carried out by the SACLANT ASW Research Centre between the end of 1959 and the end of 1964.

The reports are based mainly on a number of Technical Notes distributed only within the Centre itself. Short reports of current work have appeared regularly in the Centre's Quarterly Status Reports and, on occasions, in briefing material for various Scientific Committees. However, the present series is the first comprehensive description of the research carried out in this field by the Centre.

Naturally, as in all scientific work, some work that was started turned out to be less fruitful than expected. In addition, the departure of scientists studying particular fields has brought those aspects of the work to an end. For example, work on a magnetometer based on nuclear magnetic resonance, which had shown some promise, had to be discontinued for this latter reason. In order to maintain continuity, a number of such inconclusive or uncompleted studies are omitted from these reports.

The size of the Electromagnetic Research Group did not permit a broad attack on all the problems involved, and, after an initial research period, the effort was concentrated on a few aspects. For this final summary these have been divided

into three groups — each reported separately.

The first report deals mainly with EM fields of submerged dipoles and finite antennas. A large amount of work in this field has been done by other investigators, and some of the results of this work have been used in this theoretical study. The second report deals with the EM background noise in the ELF range and the instrumentation developed for its measurement, which constituted the main part of the Centre's work on EM phenomena in the ELF range. The third report, which is classified, deals with the special applications to ASW.

The major part of the research was carried out during a period when similar work was being done in many other places. The number of published papers on the subject has increased rapidly, doubling within only the last three years. To keep track of these developments, a bibliography was prepared in 1962. Since then, the rapid increase had demanded a second edition (Ref. 1), which was published in 1964. As practically all phenomena in the ELF range are related in one way or another to phenomena outside this range, the bibliography also includes papers on geomagnetic disturbances below 1 cps and VLF phenomena above 3,000 cps. It thus contains abstracts of about 1,700 papers and is used as a general reference throughout this series. In specific cases, however, direct reference is made to the individual papers listed in each report's bibliography.

During the research period, the following scientists (listed alphabetically) have worked for longer or shorter periods in the Group.

L. Brock-Nannestad (Denmark)
Y. Faroudja (France)
K. Hansen (Denmark)
J. Marthins (Norway)

P.E. Mijnarends (Netherlands)

H. Rynja (Netherlands)

E. Sirovich (Italy)

T. Strarup (Denmark)

G. Tacconi (Italy)

The present series contains contributions from all the above, but, for clarity, the individual contributions are not presented separately and references are only made when the work has been reported in the open literature. The series of reports thus represents the work on the whole group.

The author, who has been Group Leader throughout, wishes to acknowledge the collaboration and contributions of his colleagues in this research. The main part of the work was carried out during a period in which the Centre was under the directorship of Dr. E.T. Booth and Dr. J.M. Ide, and the author expresses his thanks to them for their interest and support.

NATURAL BACKGROUND NOISE AND INSTRUMENTATION FOR ITS MEASUREMENT

ABSTRACT

The report is the second of a series of three that discusses various EM phenomena in the ELF range.

A general outline of the natural background noise in the frequency range between 1 and 50 cps is given and the measurement instrumentation developed and used by the EM Group is described.

LIST OF SYMBOLS AND ABBREVIATIONS

A	=	loop area
A_{eE}, A_{eL}	=	effective area of electrode system and loop, respectively
A_o	=	cross section of magnetic core
$A_1(t)$, $A_2(t)$	=	amplifier noise of systems 1 and 2 respectively
amp/m	=	amperes per metre
a'	=	radius of sphere
α	=	noise constant of tube
B, $\vec{B}$	=	magnetic induction
β	=	inclination of magnetic vector
C	=	noise power constant
C'	=	noise constant of tube
C_s	=	stray capacity
γ	=	unit of magnetic field-strength $1\gamma = 8 \times 10^{-4}$ amp/m $= 10^{-5}$ Oe
γ_{rms}	=	rms value of magnetic field-strength measured in γ
γ_1	=	intrinsic propagation constant of conducting medium
d_o	=	diameter of magnetic core
Δf	=	frequency bandwidth
$\Delta\varphi$	=	phase difference
δ	=	skin-depth
E_{DC}	=	DC potential between electrodes
$E_{N,q}$, $E_{N,s}$	=	noise voltages of electrodes
E_h	=	horizontal electric field-strength

$E_1(t)$, $E_2(t)$ = electrode noise of systems 1 and 2, respectively

e, e_1 = voltage induced in metal-cored coil

e_F = flicker noise voltage

e_{iE}, e_{iL} = voltage induced in electrode system and loop respectively

e_oE, e_{iL} = open circuit voltage of electrode system and loop respectively

e_T = transistor noise voltage

f = frequency

f_1, f_2 = frequency band limits

f_m = mean frequency

f', f_1', f_2', f_{12}' = rms values of signal and noise sources

$f_1(t)$, $f_2(t)$ = output functions of channels 1 and 2 respectively

G_1, G_2 = antenna gains

G_{rE}, G_{rL} = relative gains of electrode system and loop, respectively

η = intrinsic characteristic impedance

H_h = horizontal magnetic field-strength

θ, θ_o = angles of rotation

J_1, J_1' = input currents

J_2 = output current

i_N = noise current

i_s = signal current

i_T = transistor noise current

in/sec = inches per second

k = degrees of freedom

k_o = free space wave number

L, L_o, L_1	=	inductance of coils
ℓ	=	length of electrode system
ℓ_{eE}, ℓ_{eL}	=	effective length of electrode system and loop respectively
ℓ_o	=	length of magnetic core
μa	=	microampere
μ_{ac}	=	permeability in presence of AC field
μ_i	=	initial permeability
μ_o	=	free-space permeability
μOe	=	micro-oersted
μ_r	=	rod relative permeability
μv	=	microvolt
mv	=	millivolt
mvpm	=	millivolts per metre
mho	=	unit of conductivity
ms	=	millisecond
N	=	number of turns in coil
$N_1(t)$, $N_2(t)$	=	noise of channel 1 and 2 respectively
n	=	number of turns in loop
Oe	=	oersted (see γ)
P_{N2}	=	output noise power
P_{rec}	=	received power
P_{S2}	=	output signal power
P_{trans}	=	transmitted power

R	=	distance between transmitter and receiver
$R\rho$	=	feedback resistance
R_{rE}, R_{rL}	=	radiation resistance of electrode system and loop respectively
R_s	=	series resistance
r_o	=	radius of magnetic core
$S_c(t)$, $S_u(t)$	=	coherent and incoherent part of signal
s, s_o	=	lateral displacement
σ	=	conductivity of rod material
σ_1	=	conductivity of lower medium
T_n	=	sample length
t	=	time
τ	=	time delay
U_1, U_1'	=	input voltages
U_2, $U_2^{(1)}$, $U_2^{(2)}$, $U_2^{(3)}$, $U_2^{(4)}$	=	output voltages
vpm	=	volts per metre
W_e	=	effective filter bandwidth
w-sec	=	watt-second
Y_A	=	admittance of load
Y_I	=	input admittance of amplifier
Y_p	=	feedback admittance
Y_s	=	source admittance
$Y_{11}, Y_{12}, Y_{21}, Y_{22}$	=	coefficients of Y-matrix of amplifier

$\varphi_{11}(\tau)$, $\varphi_{22}(\tau)$ = auto-correlation functions

$\varphi_{12}(\tau)$ = cross-correlation function

$\varphi_{SSc}(\tau)$, $\varphi_{SSu}(\tau)$ = auto-correlation function of coherent and incoherent part of signal respectively

$\varphi_{NN1}(\tau)$, $\varphi_{NN2}(\tau)$ = auto-correlation function of noise

ω = angular frequency

INTRODUCTION

The knowledge of EM background noise in the frequency range 1 - 50 cps has increased rapidly during the past five years. This is illustrated by the number of papers published on this and related subjects (Ref. 1), as shown by the graph in Fig. 1. This covers the open literature on EM phenomena in the frequency 1 - 3000 cps and includes many papers on geomagnetic phenomena and VLF.

Research on EM phenomena started at this Centre at the end of 1959. It was obvious from the beginning that it was necessary to gather information on the background noise in the frequency range of interest, and the first two years were spent on the development of the instrumentation required and on preliminary measurements.

The Italian Navy permitted the erection of two measuring stations on the island of Tino in the Gulf of La Spezia (Figs. 2 and 3), and most of the preliminary measurements were made on this island. As the island is uninhabited, it was possible to switch off the power to the island and thereby reduce the power-line noise that generally hampers the measurements of the natural background noise.

The measurements were made in air with solid metal-cored horizontal coils, which will be described in a later section. The main disadvantage was that these had an unpleasant transfer-function and also required a very high platform stability. Since one of the main projects was to measure the noise at sea, the island station was abandoned for some time and emphasis was put on the measurement of the horizontal electric field at short distances below the sea surface. This equipment will also be described in a later section.

Recently the stations on Tino have come into use again because of the co-operation between the Pacific Naval Laboratory, Esquimalt, B.C., Canada, and this Centre on world-wide coherence in the ELF range. The equipment installed at the stations for this purpose is of Canadian design and measures all three components of the time-derivative of the magnetic field variations.

The study of background noise given in this report is based on various published papers and on the measurements made by the EM group. There is generally reasonable agreement between the results obtained by various investigators, but a direct comparison can sometimes be difficult due to the lack of standardisation of the instrumentation and because measurements can be influenced strongly by local geological conditions. Most other measurements have been made on land, whereas the EM Group has concentrated on measurements at sea. This also tends to make a comparison difficult in some cases.

The instrumentation used by different investigators varies considerably and has often been developed from equipment used for other purposes. Also, the equipment used by the EM Group has had a certain evolution, and the result reached at the time of writing is not considered as a final and optimum solution. The description will show the basic ideas behind the equipment and how an experimental set-up was put together.

1. EM BACKGROUND NOISE

The background noise in the frequency range of interest, 1 - 50 cps, is due to sources of different origin. Around 1 cps, and occasionally up to 3 - 5 cps, the noise energy is dominated by geomagnetic effects of the micropulsation type, whereas the rest of the range is dominated by world-wide thunderstorm activity.

1.1 Geomagnetic Micropulsations

Generally, geomagnetic micropulsations can be divided into two categories: impulsive and regular. The impulsive type contains a fairly broad band of frequencies. It commences and stops abruptly and has a great dynamic range. The frequency of occurrence and the amplitude are latitude-dependent, with the higher values in the auroral zones. The regular type of micropulsations generally consists of groups of pulsations of nearly sinusoidal character. Their dynamic range is smaller than that of the impulsive type. They grow up and die away at a slow rate and can be present for time intervals of many minutes.

These phenomena have been observed by many investigators all over the world and their diurnal and seasonal variations have been determined. Their correlation with other EM-phenomena, solar activity, etc. has been noted and several theories have been put forward as explanations for the generating mechanism.

It is generally accepted that the pulsations are generated in the upper atmosphere and exosphere due to the trapping of charged particles in the earth's magnetic field. The propagation of these pulsations is assumed to be by hydromagnetic waves through the ionosphere. This generating and propagating mechanism would apply for micropulsations with frequencies between 0.5 and 5 cps, and can explain most of the observed phenomena.

Observations and interpretations of micropulsations are generally carried out by visual waveform studies. The classification of the different types of micropulsations is made difficult by the lack of a standard notation. Furthermore, the equipment used by different investigators varies, which makes comparison (which is based on published papers), extremely difficult, since the characteristics of the instruments influence the waveshape considerably. The waveform of a phenomenon looks quite different when observed with, for example, a total field magnetometer, a component magnetometer, induction coils or earth current equipment. The only parameter common to all investigators is the time scale, which makes it possible to study coherency, frequency of occurrence, etc. Moreover, there does not seem to be much point in presenting figures of typical events.

Only recently, the technique of power spectrum analysis has been introduced into the research in the micropulsation range, and seems to throw new light on some of the problems. Since some of the observed phenomena are due to non-linear transmission media, it is expected that a better understanding can be obtained by bispectral analysis (Ref. 2).

Absolute levels of the background noise in the micropulsation range are found in relatively few published papers. On the basis of a number of papers (Ref. 3 for example) it seems reasonable to assume the following values for the horizontal magnetic component on land at about mid-latitude and in the frequency ranges 1 - 5 cps:

Quiet periods	$\sim 5 \times 10^{-5}$ to 10^{-4}	$\frac{\gamma \text{ rms}}{\sqrt{\text{cps}}}$
Average periods	$\sim 5 \times 10^{-4}$ to 10^{-3}	"
Disturbed periods	$\sim 10^{-3}$ to 10^{-2}	"

($1\gamma = 8 \times 10^{-4}$ amp/m is a frequently used unit in geomagnetic research.)

As already mentioned, the levels will depend on the latitude, but the horizontal components should theoretically not be greatly affected by the nearness of a conductivity discontinuity. This has been verified experimentally within a factor of about 2.

1.2 Worldwide Thunderstorm Activity

The other part of the spectrum is dominated by the worldwide thunderstorm activity and the earth ionosphere cavity resonance. The modes of oscillation in the cavity were first discovered by Schumann in 1954. The excitation of the modes and the propagation in the cavity has been dealt with by a large number of investigators. Basically, the phenomena are well understood, and the variations with the height and condition of the ionosphere have been explained fairly well. The level of the mode frequencies, of which the lowest is about 7.5 cps, is fairly stable with diurnal variations. A variation of a factor of two in amplitude is considered large and changes occur at a slow rate. Variations with the season of the year have been noted.

A graphic recording of the noise in this frequency range looks like "short cut grass", with a number of bursts of a few cycles duration and with amplitudes of several times that of the "grass". These bursts are apparently coherent over most of the earth. Apart from these coherent bursts, local thunderstorm activity will also be recorded and will enhance the noise level.

1.3 Other Sources

A third part of the background noise is formed by man-made noise and consists mainly of switching transients on power lines, sub-harmonics of power lines, etc. Disturbances of this kind are normally easily recognisable in the power spectrum.

Apart from local noise sources, the background noise does not vary drastically with latitude and geological conditions. Coastline effects are observed in certain areas — such as fjords, lochs, etc. — and in these cases the levels can vary considerably.

For the horizontal magnetic component on land within the frequency range 5 - 40 cps, the average level is of the order of:

$$H_h \sim 5 \times 10^{-4} \quad \frac{\gamma \text{ rms}}{\sqrt{\text{cps}}}$$

with possible variations of a factor of two. This value is a broad average, not taking into account the fact that the levels at mode frequencies are somewhat higher than those between these frequencies.

To conclude these general remarks, it is worthwhile mentioning that the noise levels in the 1 - 10 cps bands seem to be somewhat lower than in the adjacent bands, but probably not low enough to characterise this part of the spectrum as a window. The various phenomena, which overlap in this range, make this range interesting from a scientific point of view, and this interest has increased considerably during recent years.

2. INSTRUMENTATION FOR EM NOISE STUDIES IN THE ELF RANGE

The study of the natural background noise in the frequency range 1 - 50 cps has been approached from two directions and is characterised by the multitude of instruments used.

2.1 Measurement of Geomagnetic Micropulsation Noise

Originally, the interest in micropulsations emerged from studies of the earth's magnetic field and its variation with time and with other observable phenomena. It was natural to utilise normal station magnetometers, which could be modified to respond to higher frequencies and to have greater sensitivity. From these modifications were derived a number of instruments for stationary use.

These instruments mainly measure the total components of the earth's magnetic field and are often called component magnetometers. They measure both the DC and AC part of the field and are generally oriented along the three orthogonal directions. It is not the intention here to give a description of these instruments. Numerous papers have been published on the subject and will be found listed in the "Bibliography of EM Phenomena" (Ref. 1). Among the better known types are fluxgate magnetometers and Hall-effect magnetometers.

During recent years other types of magnetometers have become popular. These are the so-called total-field magnetometers, which measure the total vector of the earth's magnetic field. The best known of these instruments are the proton resonance, the rubidium-vapour and the metastable helium magnetometers. Of these the proton-resonance magnetometer is only suitable for frequencies below 1 cps, whereas the other two can be made to respond to frequencies up to about 10 cps or higher. All three are characterised by the fact that they measure both the DC and AC part of the total vector. Detailed descriptions of these instruments will be found in numerous papers listed in the "Bibliography of EM Phenomena" (Ref. 1).

The noise level of practically all the magnetometers is about 10 mγ , so that only part of the natural background noise can be measured with these instruments. Work is in progress to reduce the noise levels still further.

For the study of micropulsations and EM noise at higher frequencies it is of no interest to measure either the DC part or the long term variations, and to do so sometimes complicates the measurements required. Many investigators approaching the problem from the high frequency part of the spectrum have therefore been using induction coils, which actually measure $d\vec{B}/dt$ instead of $\vec{B}$. In this way only the AC part of the field is measured, and the lowest frequency is determined by the lower cross-over frequency of the coil/input circuitry. If it is desired to determine $\vec{B}$, the output can be integrated electronically. Various opinions exist about the use of $\vec{B}$ and $d\vec{B}/dt$.

In general, the induction coils are oriented along the three orthogonal directions of magnetic north, east and vertical. For the horizontal components, coils with a high permeability core and many turns are used. For the vertical component, a large loop on the ground has generally been used. The noise level in instruments of this kind is mainly determined by the input noise of the amplifier that follows the coil and input transformer. Previously the flicker noise in thermionic valves (vacuum tubes) and transistors was predominant, but recent developments in semi-conductor techniques have greatly reduced this noise source. With present day equipment the noise level is well below a value equivalent to $0.1\ \text{m}\gamma\ \frac{\text{rms}}{\sqrt{\text{cps}}}$.

Since a noise level of $10^{-3}\gamma$ has to be measured in the presence of a static field of about $50 \times 10^{3}\ \gamma$, it is clear that movements of the coils must be prevented. Ground vibration and microseism may thus play an important role in

the proper functioning of the instruments. In general, great care has to be taken in selecting sites for the measurement of pure natural background noise in the micropulsation range.

2.2 Measurement of Thunderstorm Activity Noise

In the frequency range of 5 - 50 cps most of the investigators have been using induction coils similar to those described above, but with a fewer number of turns. The problems involved are rather similar to those met in measuring geomagnetic micropulsation noise and in this case also, a careful site selection is required.

A number of investigators have preferred to measure the earth currents generated by the changing magnetic field. This method has a number of advantages because the signal can generally be of the order of μ vpm, which makes the amplifier noise less serious. The signal can easily be increased by increasing the distance between the two electrodes with which the potential difference is measured.

Naturally, the method has its drawbacks. First of all, the measuring site has to be selected with great care with respect to the geological uniformity of the ground. Stratified layers, major conductivity discontinuities, etc., can influence the amplitude and phase of the received signal in such a way that its direct connection with magnetic field variations is obscured. Secondly, the electrodes used can generate noise, especially if the ground conductivity differs greatly at the positions of the two electrodes. Generally these difficulties are overcome, and earth current equipment has been used widely. The interpretation of the received signals and their waveform can be rather complicated if one wants to compute the magnetic field variations on the basis of the electric field (Ref. 2).

For the frequencies in the cavity modes, it has been found convenient to use a short, vertical monopole antenna in air. The field strength in the cavity is of the order of 0.2 mvpm, the field being more or less vertically polarized, depending on the ground conductivity. Antennas of this kind are extremely small compared with the wavelength, and the impedance is high. By suitable design of the input circuit of the amplifier it is possible to obtain good signal-to-noise ratios for the background noise signal. The monopole is omnidirectional and cannot therefore be used to determine the direction of arrival of the background signal. If this information is wanted, it is preferable to use horizontal magnetic detectors. It is generally claimed that vibration of the vertical antenna by the wind does not influence the measurements. Rain and charged dust particles, however, can give rise to unwanted noise.

The electronic part of the instrumentation depends to a large extent on the sensor used. A detailed description will not be given here, but reference is made to the many papers describing equipment for the measurement of ELF noise (Ref. 1). In general, it is preferable to make the amplifiers broad-band and even to incorporate pre-whitening filters.

Paper records have for many years been preferred for the display of the signal waveform or the rectified and smoothed average value. This technique is suitable if time of occurrence and waveforms are studied. A more complete analysis required other recording techniques, and the availability of magnetic-tape-recorders with suitable modulation equipment or speed-up possibility now facilitates such an analysis. Analogue recording is normally used and the processing can be made by either analogue or digital electronic means. Recording in digital form would also be possible, but so far no complete digital system has been reported in the literature. Paper recording still seems widely used both for monitoring the magnetic recording and for visual selection of samples that deserve a more careful study.

3. INSTRUMENTATION DEVELOPED AND USED BY THE EM GROUP

The initial investigations in the ELF range were made with magnetic detectors, which were readily available. In the first part of this section a description of the complete measuring assembly will be given, together with the reasons why this technique was abandoned and changed to electric dipole systems.

Most of the initial measurements were made at the island of Tino in the Gulf of La Spezia. This island was chosen after several attempts to find a place where the man-made noise was as low as possible. The position of the island is shown on Fig. 2. It belongs to the Italian Navy and is not inhabitated, except for the personnel on the lighthouse. It is possible to cut off all the power from the island, and this facility has been used on several occasions when it was necessary to reduce the power-line interference to a minimum.

Originally, two stations were erected, one on the east side near the beach, the other on the west side, about 80 m above sea level. The latter functioned as the main station. Fig. 3 shows the position of the two stations. The reason for erecting two stations on Tino was the desire to learn about the coherency of the background noise. As will be shown later, the pick-up coils introduce large phase shift, which made a careful study impossible.

3.1 Instrumentation for Studies of the Horizontal Magnetic Component

A block diagram of the complete instrumentation for one channel is shown in Fig. 4. It consists of the pick-up coil with its calibrating winding, a low noise preamplifier, a 50 cps stop filter, a main amplifier and a number of display and recording units. The calibrating coil generates a known field in the pick-up coil, so that an absolute calibration can be made. The main features of the most

important parts are given below.

3.1.1 The Pick-Up Coil

The pick-up coil consists of a solid μ -metal rod with a coil surrounding it. The specifications are as follows:

Core: Solid μ -metal rod
Length, ℓ_o , = 202 cm
Cross Section, A_o = 3.8 cm^2
Ratio: length to diameter, ℓ_o / d_o = 92
Rod relative permeability, μ_r = 2,000

Coil: Number of turns, N = 25,000
Series resistance, R_s = 65 ohm
Stray capacity, C_s = 5,400 pf .

When a long rod of high μ material is placed in a homogeneous, static magnetic field, a magnetization of the rod will take place, resulting in a reduction of the permeability. The magnetization is characterised by the demagnetization factor, which depends on the shape of the rod. Bozarth (Ref. 4) showed that, for the length-to-diameter ratio of 92 and an initial permeability μ_i = 20,000, the rod permeability μ_r = 2,000.

When an AC field is superimposed on the static field, eddy currents are induced in the solid core; Kaden (Ref. 5) gives a complete treatment of the generation of eddy currents in round wires or rods. The permeability ratio is given as:

$$\frac{\mu_{ac}}{\mu} = \frac{\delta}{r_o}\left[1 - j\left(1 - \tfrac{1}{2}\frac{\delta}{r_o}\right)\right]$$

$$= \frac{\delta}{r_o}\sqrt{2 - \frac{\delta}{r_o} + \frac{1}{4}\left(\frac{\delta}{r_o}\right)^2}\,\angle \arctan\left(\tfrac{1}{2}\frac{\delta}{r_o} - 1\right) \quad \text{(Eq. 1)}$$

where r_o is the radius of the rod, and where the skin depth in the rod material is:

$$\delta = \sqrt{\frac{2}{\omega \mu_r \sigma}}$$

in which μ_r is the relative permeability, σ the conductivity and ω the angular frequency.

Equation 1 is an approximation that is valid for $r_o \geq 2\delta$. Within the range $\delta < r_o < 2\delta$ this approximation estimates the real part about 10% too low and the imaginary part about 20% too low. For the range $r_o < \delta$, a better approximation is given by:

$$\frac{\mu_{ac}}{\mu} = 1 - j\frac{1}{4}\left(\frac{r_o}{\delta}\right)^2$$

$$= \sqrt{1 + \frac{1}{16}\left(\frac{r_o}{\delta}\right)^4} \angle \arctan\left[-\frac{1}{4}\left(\frac{r_o}{\delta}\right)^2\right] \quad \text{(Eq. 2)}$$

In the present case r_o = 11 mm. The material has a conductivity of 1.6×10^6 which, with μ_r = 2,000, gives a skin depth

$$\delta = \frac{22}{\sqrt{\omega}} \text{ mm}$$

Thus

$$\frac{\delta}{r_o} = \frac{2}{\sqrt{\omega}}$$

The voltage induced by the AC-field in the coil is given by:

$$e = \omega \cdot B \cdot A \cdot N \cdot \mu_r \cdot \frac{\mu_{ac}}{\mu}$$

$$= \omega \cdot B \cdot A \cdot N \cdot \mu_r \cdot \frac{2}{\sqrt{\omega}} \sqrt{2 - \frac{2}{\sqrt{\omega}} + \frac{1}{4}\left(\frac{2}{\sqrt{\omega}}\right)^2} \angle \arctan\left(\frac{1}{\sqrt{\omega}} - 1\right)$$

$$= B \cdot A \cdot N \cdot \mu_r \cdot 2\sqrt{2\omega - 2\sqrt{\omega} + 1} \angle \arctan\left(\frac{1}{\sqrt{\omega}} - 1\right) \quad \text{(Eq. 3)}$$

where B is the induction.

It is seen that both the amplitude and phase of the induced voltage vary with $\sqrt{\omega}$.

The amplitude of the induced voltage can thus be expressed as:

$$e = e_1\sqrt{\omega} \qquad \text{(Eq. 4)}$$

where the numerical value of the factor e_1 is that of the voltage induced when $\omega = 1\ \text{sec}^{-1}$. This factor has been computed as:

$$e_1 = 1.6 \left[\frac{\mu v}{\mu\ 0e\ \text{sec}^{1/2}}\right]$$

The self-inductance of the pick-up coil is given by:

$$L = L_o \mu_r \cdot Re\left(\frac{\mu_{ac}}{\mu}\right)$$

$$= L_o \cdot \mu_r \cdot \frac{\delta}{r_o}$$

$$= L_o \cdot \mu_r \cdot \frac{2}{\sqrt{\omega}} \qquad \text{(Eq. 5)}$$

where L_o is the self-inductance of the coil without its core.
Similarly, the self-inductance can be expressed as:

$$L = L_1 \cdot \frac{1}{\sqrt{\omega}} \qquad \text{(Eq. 6)}$$

where the numerical value of the factor L_1 is that of the inductance at $\omega = 1\ \text{sec}^{-1}$. This factor has been computed as:

$$L_1 = 715 \left(\frac{\text{H}}{\text{sec}^{1/2}}\right)$$

The equivalent circuit for the pick-up coil is shown in Fig. 5. The output voltage across the load resistance Rp can be computed with the help of Eqs. 4 and 6; Fig. 6 shows both the computed and measured frequency responses for three values of load resistance. The agreement between the curves is reasonable, considering that the characteristics of the magnetic material are known only approximately.

It is seen from the curves that a response that is nearly independent of frequency can be obtained by loading the coil with a resistor of 2 kohm or less. However, a more favourable signal-to-electronic-noise ratio can be obtained by operating without a load and providing proper equalization after amplification.

The experimental frequency response was obtained by superimposing a known field on the coil. This was done with a single layer solenoid or helix. Fig. 7 shows the mechanical layout of the pick-up coil assembly, together with the calibration coil. This coil is fed with a constant current and produces a field of 0.625 $\mu Oe/\mu a$.

The main coil is surrounded by an electrostatic shield, which is connected to the outer conductor of the coaxial signal cable. The calibration coil is outside the shield, and is wound on a plastic tube having a spiral groove on its surface to keep the turns in a fixed position. This electrical system is housed in a larger plastic tube having watertight end-caps and watertight feed-throughs for the signal and calibration cables. For further protection, this complete detection system is placed on soft foam rubber material inside a concrete tube cemented to the rock about 20 m from the measuring station. In spite of these precautions, false signals due to vibration have been observed at frequencies of 1 - 2 cps. As already mentioned, the movements required to generate signals of the same magnitude as the background noise are very small and can very well be caused by microseisms.

3.1.2 The Preamplifier

The requirements for the preamplifier are given by the previously mentioned signal levels and the equivalent circuit for the pick-up coil. The low signal level requires an extremely low-noise amplifier and, as the amplifier has to be battery operated, it was thought that a transistor amplifier would be suitable. Such an amplifier was designed and tests were carried out, but it was found that, with the transistors available at that time, it was not possible to fulfil simultaneously the requirements of both low noise and high dynamic range in the input stage of the amplifier. Due to the developments in semi-conductor design this situation is now changed, and today it is possible to design a transistorized, low-noise amplifier for the required frequency range and with adequate dynamic range. For the sake of continuity, however, a brief description of the thermionic valve amplifier that was developed will be given.

The main noise-source in the frequency range of 1 - 100 cps is the so-called flicker-noise, which is present both in valves and semi-conductors. For valves, the flicker-noise voltages can be expressed by:

$$\overline{e_F^2} = \left(\frac{C'}{f_m^{\alpha}}\right)^2 \Delta f \qquad \text{(Eq. 7)}$$

where C' and α are so-called "constants" determined by the construction of the valve, the cathode material, the working conditions, etc., Δf is the bandwidth $f_2 - f_1$, and

$$f_m = \frac{f_2 - f_1}{\log_e \frac{f_2}{f_1}} \qquad \text{(Eq. 8)}$$

Very often it is assumed that $\alpha = 0.5$, in which case Eq. 7 expresses the well-known 1/f law.

For a critical design, however, this assumption is not good enough. Only a few manufacturers publish adequate information of the flicker-noise behaviour of valves. A paper published by Rothe (Ref. 6) gives data on the Telefunken valve EF 804 and gives a design procedure for low noise amplifiers. With the recommended working point, the noise constants are given as:

$$C' = 10^{-6} \text{ and } \alpha = 0.71$$

In a frequency range of 1 - 100 cps, with $f_m = 21.5$ cps and $\Delta f = 99$ cps, Eq. 7 gives:

$$\overline{e_F} = 1.16 \, \mu v_{rms},$$

which refers to the input of the valve. For comparison, it can be mentioned that this corresponds to the thermal noise of a 2.7 megohm resistor at the input of the valve.

This noise voltage can be reduced by coupling a number of valves in parallel. Since there is no correlation between the noise of one valve and another, the noise power will decrease proportionally with the number. Five parallel valves were chosen as a compromise between noise reduction and power consumption, which is of importance in battery-operated equipment. With the above-mentioned noise-voltage and bandwidth this would correspond to an input noise of $23 \times 10^{-9} \; v_{rms}/\sqrt{\text{cps}}$.

In addition to this noise there are other noise sources, such as microphonics, resistance noise, battery noise, thermo-electric noise, etc. On the final version of the preamplifier, the circuit diagram of which is shown in Fig. 8, an equivalent noise voltage of 40×10^{-9} $v_{rms}/\sqrt{cps}$ was measured with 65 ohms at the input. This is in reasonable agreement with the computed value, especially because the working point had to be changed from its optimum because of the available battery voltage.

By comparing this noise voltage with the measured output of the pick-up coil as shown in Fig. 6, the minimum measurable field can be determined. At, for example, 10 cps, 40×10^{-9} $v_{rms}/\sqrt{cps}$ corresponds to 1.3×10^{-9} 0e or 0.13 m$\gamma_{rms}/\sqrt{cps}$. A 1 mγ signal can therefore be measured with a signal-to-noise ratio of about 8.

The amplification of the amplifier in Fig. 8 is 180, with a flat frequency response between 1 and 200 cps. The dynamic range was measured to about 100 db, which was adequate for operating the amplifier directly on the pick-up coil without power line filter or other circuitry in front of the amplifier. In the mechanical lay-out, great care was taken to reduce microphonics and influence from outside sources. The amplifier was housed in a screened, air-tight box with a separate box for the battery power supply.

3.1.3 Power-Line Filter and Main Amplifier

Between the preamplifier and the main amplifier it was usually necessary to have a stop filter for the power line frequency. The filter was designed around a bridged-T notch network with a tunable inductance. The circuit is shown in Fig. 9. The filter is tuned in steps of 0.5 cps within the range 48 - 52 cps; a minimum attenuation of 26 db is obtained in this range, but generally the attenuation is much larger.

The main amplifier was designed around a direct-coupled transistor pair and consisted of one or more sections. The circuit diagram of one of these sections is shown in Fig. 10. The amplification is determined by the feedback resistors of 1 and 22 kohm respectively. The DC-feedback stabilizes the working point and, with the components shown, the lower cross-over frequency was 0.2 cps. At the high frequency end, the frequency response can be changed by the condenser C, which is shown in dotted lines across the 22 kohm resistor. Without the condenser the response is flat up to about 70 kc, depending on the transistors. The other specifications are: voltage gain 20 (26 db), input impedance 50 kohm, output impedance 1.5 kohm, open circuit output voltage 3.5 v_{rms}, noise referred to input max. 4 $\mu v_{rms}/\sqrt{cps}$ (which is lower than the amplified noise from the preamplifier). The power consumption is 3 ma at 18 v. Altogether it has proved itself to be a very versatile general purpose amplifier. A number of sections operating off separate batteries have been constructed in screened boxes; these have been used widely whenever a signal level had to be raised for the sake of a particular experiment.

As is seen from the block diagram (Fig. 4), the main amplifier is followed by a number of recording and display instruments which, except for the tape recorder, are of commercial design. All these instruments had sufficiently high input impedance to operate without a power amplifier.

3.2 Instrumentation for Studies of the Horizontal Electric Component at Sea

3.2.1 General

One of the objectives of the research programme was to study the electromagnetic background noise at sea, far from man-made noise and coastlines and with cleaner geometry than could be obtained on land. However, the experience gained with

the equipment just described showed that it would not be possible to use the magnetic detector in its existing form from a floating platform, because the pick-up coil's sensitivity to vibrations made it unlikely that it could be suspended in such a way that its movements within the earth's static magnetic field would be negligible.

This was solved by measuring the horizontal electric component in the sea close to the surface. Basically this is the same technique as is used in earth current measurements. The relation between teluric currents and the earth's magnetic field has been treated by Wait (Ref. 7) for the general case.

As a first approximation one has the simple relation between electric and magnetic field strength:

$$E_h = \eta \cdot H_h \qquad \text{(Eq. 9)}$$

where η is the complex, intrinsic, characteristic impedance of the lower medium — in this case the sea. This is expressed as:

$$\eta = \frac{i\mu_o\omega}{\gamma_1} \qquad \text{(Eq. 10)}$$

where $\gamma_1^2 = i\sigma_1\mu_o\omega$ is the intrinsic propagation constant of the lower medium when displacement currents are neglected, and where σ_1, μ_o and ω are the conductivity, permeability and frequency respectively.

Introducing the expression for γ_1 one obtains:

$$\eta = \frac{\sqrt{\sigma_1\mu_o\omega}}{\sigma_1} \angle\frac{\pi}{4} \qquad \text{(Eq. 11)}$$

With σ_1 = 4 mho/m, $\mu_o = 4\pi \times 10^{-7}$ H/m and $\omega = 2\pi f$, the impedance is $\eta = 1.4 \times 10^{-3} \sqrt{f} \angle \frac{\pi}{4}$ ohm and the relation between the modulus of the electric field-strength and the modulus of the magnetic field-strength is:

$$E_h = 1.4 \times 10^{-3} \sqrt{f} \cdot H_h \qquad \text{(Eq. 12)}$$

The phase relationship has not been considered here. E_h is expressed in vpm if H_h is measured in amp/m. For a background noise field of about 1 mγ = $= 8 \times 10^{-7}$ amp/m one would obtain:

$$E_h = 1.13 \times 10^{-9} \sqrt{f} \text{ vpm}$$

Preliminary measurements were carried out with a 100 m long floating cable and two stainless steel electrodes. Experiments showed that the technique was feasible even if a number of new noise sources were observed. Naturally, in this case also, the movements of the dipole in the earth's magnetic field introduced unwanted signals. Noise due to the electrodes themselves was also observed. The general result was, however, interesting enough to continue the work and to try to reduce some of the noise sources.

Before going into a detailed description of the development of the electrode system, it is worth looking into the relative merits of loops and electrode systems as pick-up devices for electromagnetic background noise and at their behaviour during movements.

3.2.2 Comparison Between Electrode Systems and Loops

In the theoretical comparison between electrode systems and loops the following conditions are assumed. Both receiving systems are assumed to be immersed in a semi-infinite medium, whereas the EM field, from which the signal energy

has to be extracted, is generated in the medium above the boundary. The source is assumed to be far away and the field to be vertically polarized. Below the boundary, however, both electric and magnetic fields will be horizontal.

Following Hansen (Ref. 8), the problem will be approached on the basis of general antenna theory, which is strictly valid only for far fields. For the frequencies involved in ELF the range dependence of the field-strength corresponds to an intermediate region, and only a rough approximation is given by the standard range equation:

$$\frac{P_{rec}}{P_{trans}} = \frac{G_1 \cdot G_2}{4k_o^2 \cdot R^2} \qquad \text{(Eq. 13)}$$

where G_1 and G_2 are the gains of the transmitting and receiving antenna respectively

k_o is the free space wave number,

and R is the distance between transmitter and receiver .

It is assumed, however, that since no absolute field-strength calculations are made, Eq. 13 can be used for the determination of the relative merits of two antennas.

In the present case both antennas are assumed to receive the same power, so that:

$$\frac{P_{rec}}{P_{trans}} = \frac{G_1 \cdot G_{rE}}{4k_o^2 \cdot R^2} = \frac{G_1 \cdot G_{rL}}{4k_o^2 \cdot R^2} \qquad \text{(Eq. 14)}$$

where G_1 is the gain of the transmitting antenna and G_{rE} and G_{rL} are the relative gains of the electrode system and loop respectively. It follows from Eq. 14 that:

$$G_{rE} = G_{rL} \qquad \text{(Eq. 15)}$$

As has been shown by Wait (Refs. 9 and 10), a loop is most efficiently employed if it is embedded in an insulating sphere. The electrode system therefore is compared with such a loop and the relative gains given by Ref. 8 can be used, so that:

$$G_{rL} = \frac{3}{4} k_o^3 a' \delta^2 \qquad \text{(Eq. 16)}$$

$$G_{rE} = \frac{4}{\pi} k_o^3 \ell \delta^2 \qquad \text{(Eq. 17)}$$

where
- a' = radius of sphere (radome)
- ℓ = length of electrode system
- δ = skin-depth

Eq. 15 is fulfilled if:

$$a' = \frac{16}{3\pi} \ell = 1.7 \ell \qquad \text{(Eq. 18)}$$

The above treatment is similar to Wheeler's small antenna concept, which states that the performance of a small antenna should be roughly proportional to the volume occupied. This would lead to $a' \approx \ell$, instead of as in Eq. 18.

A condition has thus been found under which the two antennas will extract the same energy from the given EM-field. If this condition is fulfilled, the

effective areas A_e of the two antennas will be the same, and therefore the available power will be the same. The effective length ℓ_e of an antenna expresses the open circuit voltage available at the antenna terminals and, in this case, with AeL = AeE, one obtains:

$$\frac{\ell_{eL}}{\ell_{eE}} = \sqrt{\frac{R_{rL}}{R_{rE}}} \qquad \text{(Eq. 19)}$$

where R_{rL} and R_{rE} are the radiation resistances of the loop and the electrode systems respectively. Introducing the expressions given in (Ref. 8) for R_r, and applying Eq. 18, one obtains

$$\frac{\ell_{eL}}{\ell_{eE}} = \frac{A\,n}{\delta\,\ell\sqrt{2}} \qquad \text{(Eq. 20)}$$

where A = loop area

n = number of turns.

Equation 20 expresses the degree of freedom in the design of the two antennas. For the electrode system there is only one parameter, ℓ, whereas the loop has two, namely the area A and the number of turns n. For an air-core loop the maximum area is given by a', as specified in Eq. 18. By utilizing magnetic material, A can be increased, and thus the open-circuit voltage can also be increased. It should be noted, however, that this does not change the gain of the antenna or the available power, and is thus only an impedance transformation of the radiation resistance, which naturally requires another load resistance for optimum power transfer.

Before leaving Eq. 20, the voltages induced in both a loop and an electrode system will be computed for the case where they are moving in the earth's static magnetic field. There is a fundamental difference between the two devices in this case. For the electrode system a voltage will be induced by a lateral

displacement, whereas a turning displacement is required to induce a voltage in the loop. In comparing the two systems it is assumed that the electrode system is displaced by a length s in the horizontal plane and that the radome loop is turning through a small angle θ around a horizontal axis. Both movements are supposed to be periodic, with an angular frequency ω and with the respective amplitudes s_o and θ_o.

When B is the DC-component of the earth's magnetic field and β is the inclination, then the voltage induced in the electrode system is:

$$e_{iE} = \ell \frac{ds}{dt} B \sin\beta \qquad \text{(Eq. 21)}$$

When

$$s = s_o \sin \omega t$$

is introduced

$$e_{iE} = \ell s_o \omega B \sin\beta \cos \omega t \qquad \text{(Eq. 22)}$$

Similarly for the loop, the flux through the loop is:

$$\Phi = n A \theta B \sin\beta \qquad \text{(Eq. 23)}$$

and with

$$\theta = \theta_o \sin \omega t \quad ,$$

$$|e_{iL}| = \frac{d\Phi}{dt}$$

$$= n A \theta_o \omega B \sin\beta \cos \omega t \qquad \text{(Eq. 24)}$$

The ratio between the two induced voltages is therefore:

$$\frac{e_{iL}}{e_{iE}} = \frac{A\, n\, \theta_o}{\ell\, s_o} \qquad \text{(Eq. 25)}$$

The effective length ℓ_e is a measure of the open circuit signal voltage available at the terminals. The term e_i is a noise voltage induced due to movement. By combining Eq. 20 with Eq. 25, a relation between the signal-to-noise voltages in the two cases can be found.

Dividing Eq. 20 by Eq. 25 yields:

$$\frac{(\ell_{eL}/e_{iL})}{(\ell_{eE}/e_{iE})} = \frac{s_o}{\theta_o} \cdot \frac{1}{\delta\sqrt{2}}$$

or

$$\frac{\ell_{eL}}{e_{iL}} = \frac{s_o}{\theta_o} \cdot \frac{1}{\delta\sqrt{2}} \left(\frac{\ell_{eE}}{e_{iE}}\right) \qquad \text{(Eq. 26)}$$

Under the given condition that the same signal power is extracted from the EM-field, Eq. 26 shows that the ratio between the signal-to-noise ratios is independent of the area of the number of turns of the loop and of the length of the electrode system.

The radiation resistance of both devices if extremely small at the low frequencies involved. In a practical system the loss resistance is appreciably higher, and from a receiving point of view it will be difficult to extract the available power from the EM field. Under these circumstances, a comparison between loops and electrode systems should not be made on the basis of general antenna theory, but rather by treating both devices as field probes.

If the horizontal electrode field-strength in water is E_h, then the open-circuit voltage available at the terminals of the electrode system is:

$$e_{oE} = E_h \, \ell \qquad \text{(Eq. 27)}$$

For the loop, the open circuit voltage at the terminals is given by:

$$e_{oL} = n A \omega \mu_o H_h \qquad \text{(Eq. 28)}$$

Introducing Eqs. 9 and 11, this is transformed into:

$$e_{oL} = E_h \, n A \frac{\sigma \mu_o \omega}{\sqrt{\sigma \mu_o \omega}}$$

or

$$= E_h \, n A \frac{\sqrt{2}}{\delta} \qquad \text{(Eq.29)}$$

The ratio between the two signal voltages becomes:

$$\frac{e_{oL}}{e_{oE}} = \frac{A \, n \, 2}{\ell \, \delta} = 2 \frac{An}{\delta \ell \sqrt{2}} \qquad \text{(Eq. 30)}$$

which, apart from the factor 2, is equivalent to Eq. 20.

The voltages induced in the two systems due to movements are the same as before and, using Eq. 30, the comparison between signal-to-noise voltage is:

$$\frac{e_{oL}}{e_{iL}} = \frac{s_o}{\theta_o} \cdot \frac{\sqrt{2}}{\sigma} \left(\frac{e_{oE}}{e_{iE}} \right) \qquad \text{(Eq. 31)}$$

This expression shows that, apart from the factor 2, the same relationship exists in this case as in the case of equal power extraction (Eq. 26). In both cases, θ_o is inversely proportional to δ for a given s_o and specified signal-to-noise ratios.

The field-probe model of the two devices can also be used in the following way. If, instead of equal power extraction, one requires only equal open circuit voltage, then Eq. 30 shows that:

$$A_n = \frac{\ell \delta}{\sqrt{2}} \qquad \text{(Eq. 32)}$$

which gives a freedom in the design of the loop.

As was mentioned in connection with Eq. 20, the introduction of magnetic material increases the output voltage and the impedance. If the output voltage is kept constant, this means that the physical dimensions can be decreased; the signal-to-noise voltage ratio is not changed and Eq. 31 is still valid. This method is equivalent to a reduced size air-core loop followed by a step-up transformer. A detailed comparison between air-core loops and rod antennas has been made by Silverstein (Ref. 11), without, however, dealing with the noise induced due to movements.

The main advantage of introducing magnetic material or a transformer would thus be that the physical dimensions of the loop can be chosen in such a way that the required stability can be obtained with minimum effort. Eq. 31 shows that for equal signal-to-noise voltage ratios:

$$\theta_o = \frac{s_o \sqrt{2}}{\delta} \qquad \text{(Eq. 33)}$$

In the frequency range between 1 and 50 cps, δ in sea-water varies between 250 m and 35 m respectively. If, for example, at 4 cps, with δ = 125 m., a displacement s_o = 1 cm is permitted, then, according to Eq. 33, $\theta_o = 113 \times 10^{-6}$ radians = 23.3 sec of arc. This is a rather strong requirement.

In the above treatment, only noise due to movements has been taken into account. For the electrode system there is, however, one noise source which must not be overlooked. This is due to electro-chemical action between the electrodes and the water surrounding them. Theoretically, this noise source is independent of the length of the system, and could be made negligible with respect to the signal by increasing the length ℓ . However, in a practical situation the length is limited by the need to reduce movement in the system. For a final selection between loops and electrode systems the following comparison of their characteristics can be made:

(1) The loop requires a much higher platform stability than the electrode system;

(2) The loop has less inherent noise then the electrode system.

An investigation of electrode material, shape and protection, however, showed that the electrode noise could be reduced considerably with fairly simple methods. Details will be given in a later section. As a result of this investigation the electrode system was selected, and an experimental model was designed.

3.2.3 Studies of Electrode Noise

Initial experiments with electrode systems indicated that noise was generated by the interaction between the electrode and the sea-water. A study was made to obtain an understanding of the mechanism and to find means to avoid the noise.

A number of tests were carried out in the laboratory to obtain a relative comparison between various electrode materials. The measurements were made in a small tank containing sea-water, in which the electrodes, consisting of metal sheets, 3.5 x 4.5 cm^2, were submerged. For each pair of electrode material, the following characteristics were measured:

(1) The D.C. potential, E_{DC}

(2) The noise voltage, $E_{N,\,q}$, in the range 2 - 32 cps, with the water in the tank completely still.

(3) The noise voltage, $E_{N,\,s}$, in the range 2 - 32 cps, when the water in the tank was stirred.

(4) The impedance, Z_p, between the plates, in the frequency range 1 - 1,000 cps.

The values obtained are represented in Table 1.

TABLE I

COMPARISON OF ELECTRODE MATERIALS

Material	E_{DC} (mv)	$E_{N,\,q}$ (μv_{pp})	$E_{N,\,s}$ (mv_{pp})	Z_p (ohms)			
				1 cps	10 cps	100 cps	1,000 cps
Stainless Steel	90	0.5	30	200	60	25	19
Monel	34	"	2	210	40	19	12
Aluminium	230	"	20	720	200	115	35
Aluminium Alloy	5	"	25	700	240	100	30
Bronze	6	"	2	160	50	15	12
Zinc	8	"	3	18	14	13	11
Carbon	25	"	2	450	70	15	10

The geometry of the experiment was the same in all cases; the only varying parameter was the material of the electrodes. The results can be interpreted

in the following way. The noise measured in still water was practically the same for all materials, and was independent of the DC potential between the plates. The noise due to corrosion on the surface was small compared with the noise due to moving water, and can therefore be neglected.

The impedance between the plates increases with decreasing frequency. This can be interpreted as a polarization effect, in which the ions form a space-charge layer around the electrodes, resulting in a potential barrier. At high frequencies the polarization is negligible, due to the low movability of the ions.

The presence of the polarization layer can also explain the large noise voltage measured when the water is stirred. The water flowing along the electrode surfaces destroys the layer, which the electrodes try to regenerate. This mechanism gives rise to moving charges which are measured as noise.

From the interpretation of Table 1, it is clear that zinc would be the best choice from the materials studied. The polarization effect is nearly the smallest and the impedance does not vary much with frequency. This latter fact is of importance for the design of the amplifier following the electrode system.

The measurements further showed that it was important to prevent the movement of water along the electrode surfaces. The same conclusion can be drawn from a report by Johnson, Orr and Zenel (Ref. 12). In order to find a simple solution to this problem, new tests were carried out. In these tests a short electrode system was built into a plastic tube of 5 cm diameter. The separation between the electrodes was only 20 cm, so that the voltage induced — due to the system's movement in the static magnetic field — could be neglected. Extension tubes of various lengths, containing various filter material, could be screwed on to the ends of the basic plastic tube. The whole system was suspended in a large tank, and the noise due to movement of the system through the water was measured.

It was shown that it was possible, with a proper thickness of gauze in front of the electrodes, to reduce the noise due to water movements to a level below the noise of the amplifier used for the tests. It was later shown that the gauze filter was also extremely effective when tried with a more sensitive amplifier. A drawback to the system is that a large gauze filter — and any other water filter — will increase the impedance of the electrode system at low frequencies. In the design of an experimental electrode system for use at sea, a compromise must be found between the electrode noise and the amplifier. The variables that determine the final result are the area of the electrode and the dimensions of the gauze-filter. As the length of the electrode system determines the signal strength, the system should be made as long as possible commensurate with platform stability and handling ease. The impedance of the electrode system is, as shown, determined by the electrodes and the filter, because the impedance of the sea is extremely small.

3.2.4 An Experimental Low-Noise Electrode System

The first, experimental electrode system, based on the findings described in the previous section, was a simple scaled-up design with a 2 m. long plastic tube. Tests were carried out at sea and these showed that the impedance had to be reduced and that a proper suspension system had to be found. The experience gained led to the design of the second experimental version described here.

The electrode system requires a rigid support to ensure that the cable connecting the two electrodes maintains a straight line and does not create magnetic loops. The presence of such loops would result in voltages induced by the rotation of the electrode system around its axis. A plastic tube of 5 m. length, with internal and external diameter of 295 and 315 mm. respectively, was found suitable for this purpose, and the rest of the device was adapted to this tube (Fig. 11.). A cross-section of the design is shown in Fig. 12.

Each electrode is a spirally-wound 30 cm x 2 m sheet of 0.5 mm thick zinc held in place by a spirally-cut,transversal, plastic disc former that retains a 24 mm gap between each of the turns. The outer edge of this plastic disc fits tightly into the inner circumference of the plastic tube. Fig. 13a shows one of the electrodes before being fitted in the tube; Fig. 13b shows the tube from one end, with the electrode in place.

The large surface of the electrodes reduces the influence of polarization on the impedance of the electrode system. As each electrode is glued into its plastic disc , which, in turn, is glued into the tube, there is no uncontrolled exchange of water between the two sides of the wall. Provision for water exchange is made through three small plastic tubes at the circumference of the spiral-disc. During submersion, the inner space is filled with water coming through these tubes and air escapes through small holes on the top of the large plastic tube. Internal screens direct the waterflow away from the electrodes, so that any exchange of water between the sea and the inner space, which could be caused by movement, does not disturb the water around the electrodes. The ends of the outer tube are provided with a cap, consisting of two perforated plastic discs with a layer of gauze between them. Practical experiments showed that a 1 mm thick layer of gauze was sufficient for protection against impurities and water movements. The flow of water is very slow and it takes 15 mins to fill the tube.

The cable connecting the electrodes with the output terminal — which is at the midpoint of the plastic tube — consists of an insulated copper wire with a lead cover, which is further insulated by a thick plastic cover. The cable is positioned along the axis of the tube by supports, and the lead cover reduces vibrations of the wire between the supports which would otherwise induce undesired voltages.

Once these precuations have been taken against electrode noise, the most serious noise source becomes the movement of the whole system in the earth's static magnetic field. From Eq. 22 it can be found that in order to measure a voltage of 10^{-9} v_{rms} the displacement of the system must, theoretically, be smaller than about $10^{-3}/f$ mm. The system thus requires a proper suspension to attenuate the movements of the platform. Fig. 14 shows a sketch of the suspension used. A 5 m long, closed, plastic tube floats at the surface and supports the electrode system with a pair of shock cords about 10 m long. With this system the movements of the floater are attenuated by a factor calculated to be of about $324\ f^2$. The resonance frequency of the mechanical system is about 0.05 cps, which, for wind speeds lower than about 25 knots, is more than one octave below the peak of the wave energy. Even with this rather high attenuation, the theoretical limit for the movements is not reached, and one would thus expect severe disturbances from the movements.

Practical tests showed, however, that the disturbances were smaller than expected. One explanation might be the following. It was supposed that the floater gave only a lateral displacement to the electrode. In practice, however, it is likely that the two points from which the cords are suspended move up and down independently. The action on the electrode system will thus mainly generate a random rotation around a horizontal axis as well as a small lateral displacement. The rotation does not, however, induce noise voltages. If this explanation is correct, then an even better system would be one in which the floater is exchanged for two spar buoys, thus permitting completely independent movement of the two support points. The shock cords will, however, still be needed for further attenuation of the movements.

A second explanation could be that the attenuation was calculated on the assumption of laminar water current around the cylinder, and, as this condition is probably not fulfilled, the actual attenuation is thereby increased.

3.2.5 An Amplifier for Electrode Systems

It was mentioned in Section 3.1.2 that the main noise source in thermionic valves and semi-conductors in the frequency range of 1 - 50 cps is the flicker noise. New developments in transistor techniques have produced transistor types that have extremely low flicker noise compared with previous types, and it was thus desirable to design a transistor amplifier utilizing these new types. A number of tests were carried out with a transistor of type 2N2484 and very good results were obtained. In contrast to previous experience with transistor amplifiers, a very high dynamic range could be maintained, even in the low-noise operating point. These encouraging results prompted the design of a complete amplifying system that would suit the electrode system.

The design of a low-noise amplifier is generally centred around the determination of the optimum source-impedance so as to obtain maximum signal-to-noise ratio at the input of the amplifier. In this section the problem will be treated for the case of a feedback amplifier, and the signal-to-noise ratio of the output will be considered.

Both the amplifier and the feedback network can be represented by their Y-matrices, as shown in Fig. 15. The next figure (Fig. 16) shows the complete circuit with all the noise sources separated, in which case the amplifier itself can be considered as noise free. It can, in general, be assumed that the different noise sources are not correlated with each other. Measurements made on the 2N2484 transistor have shown that this is a reasonably good approximation.

The relation between input and output for the amplifier is given by the following equations:

$$\left.\begin{aligned} J_1' &= Y_{11} \cdot U_1' + Y_{12} \cdot U_2 \\ J_2 &= Y_{21} \cdot U_1' + Y_{22} \cdot U_2 \end{aligned}\right\} \qquad \text{(Eq. 34)}$$

in which currents and voltages represent instantaneous values.

The output voltage U_2 will be computed for each of the sources and, with Eq. 34:

(1) $i_s = 0, \quad i_N = 0, \quad i_T = 0$

$$J_1' = J_1 = e_T \frac{Y_s \cdot Y_I}{Y_s + Y_I}$$

$$U_1' = U_1 - e_T$$

$$Y_I = Y_{11} - \frac{Y_{12} \cdot Y_{21}}{Y_{22} \cdot Y_A} = \text{input admittance of the amplifier}$$

$$U_2^{(1)} = e_T \frac{Y_s}{Y_s + Y_I} \left(- \frac{Y_{21}}{Y_{22} + Y_A} \right) \qquad \text{(Eq. 35)}$$

(2) $i_s = 0, \quad i_N = 0, \quad e_T = 0$

$$J_1' = J_1 - i_T = i_T \frac{Y_I}{Y_s + Y_I}$$

$$U_1' = U_1 = \frac{i_T}{Y_s + Y_I}$$

$$U_2^{(2)} = \frac{i_T}{Y_s + Y_I} \left(- \frac{Y_{21}}{Y_{22} + Y_A} \right) \qquad \text{(Eq. 36)}$$

(3) $i_s = 0, \quad e_T = 0, \quad i_T = 0$

$$U_2^{(3)} = \frac{i_N}{Y_s + Y_I} \left(- \frac{Y_{21}}{Y_{22} + Y_A} \right) \qquad \text{(Eq. 37)}$$

(4) $i_N = 0, \quad e_T = 0, \quad i_T = 0$

$$U_2^{(4)} = \frac{i_s}{Y_s + Y_I} \left(- \frac{Y_{21}}{Y_{22} + Y_A} \right) \qquad \text{(Eq. 38)}$$

The total noise-power at the output is given by:

$$P_{N_2} = Y_A \cdot \sum \left(U_2^{(n)} \right)^2$$

$$P_{N_2} = Y_A \cdot \left(- \frac{Y_{21}}{Y_{22} + Y_A} \right)^2 \cdot \frac{\overline{(e_T \cdot Y_s)^2} + \overline{i_T^2} + \overline{i_N^2}}{(Y_s + Y_I)^2} \qquad \text{(Eq. 39)}$$

The factor $\overline{i_N^2}$ represents the thermal noise of Y_s

and $\overline{i_N^2} = 4 k T_o \Delta f \cdot Y_s = C \cdot Y_s$ (Eq. 40)

where $k T_o = 4.1 \times 10^{-21}$ w-sec

This is introduced below in the expression for P_{N_2} (Eq. 44).

The magnitude of i_T and e_T can be determined by the measurement of the output short-circuit current with points 1-1 either open or short-circuited. In this way it is found that:

$$i_T = -\frac{Y_{11}}{Y_{21}} \cdot J_2 \qquad \text{(Eq. 41)}$$

$$e_T = -\frac{1}{Y_{21}} \cdot J_2 \qquad \text{(Eq. 42)}$$

and

$$\frac{i_T}{e_T} = Y_{11} \qquad \text{(Eq. 43)}$$

When this is introduced into the expression for the output noise, one obtains:

$$P_{N_2} = Y_A \left(-\frac{Y_{21}}{Y_{22}+Y_A}\right)^2 \cdot \frac{\overline{i_T^2}\left(\frac{Y_s}{Y_{11}}\right)^2 + \overline{i_T^2} + C \cdot Y_s}{(Y_s + Y_I)^2} \qquad \text{(Eq. 44)}$$

$$= K \frac{\overline{i_T}\left[\left(\frac{Y_s}{Y_{11}}\right)^2 + 1\right] + C \cdot Y_s}{(Y_s + Y_I)^2}$$

The optimum value of Y_s is found by the differentiation of P_{N_2} with respect to Y_s. This operation yields:

$$Y_S = Y_I \cdot \frac{2 \cdot \overline{i_T} - C \cdot Y_I}{2 \cdot \overline{i_T^2}\left(\frac{Y_I}{Y_{11}}\right)^2 - C \cdot Y_I} \qquad \text{(Eq. 45)}$$

which shows that, if $Y_I = Y_{11}$, then $Y_S = Y_I$. With the above expression for the input admittance, this condition can be fulfilled for:

$$- \frac{Y_{12} \cdot Y_{21}}{Y_{22} + Y_A} = 0$$

which is true if Y_p is chosen so that:

$$Y_p = Y'_{12} \qquad \text{(Eq. 46)}$$

With this adjustment, the output signal-to-noise ratio will be:

$$\frac{P_{S_2}}{P_{N_2}} = \frac{\overline{i_s^2}}{2 \cdot \overline{i_T^2} + C \cdot Y_s}$$

$$= \frac{i_s^2}{C \cdot Y_s} \left(\frac{1}{1 + 2 \cdot \frac{\overline{i_T^2}}{C \cdot Y_s}} \right) \qquad \text{(Eq. 47)}$$

The factor in brackets shows the influence of the amplifier, whereas the first factor expresses the ratio between the signal current and the thermal noise current from the signal source impedance. This ratio can thus be defined as the internal signal-to-noise ratio of the source itself. Since the signal can be increased by increasing the length of the electrode system without changing Y_s, the above expression shows that the output signal-to-noise ratio can be made equal to the

internal signal-to-noise ratio of the source by increasing the length of the electrode system by a factor

$$\sqrt{1 + 2 \frac{\overline{i_T^2}}{C \cdot Y_s}} \qquad \text{(Eq. 48)}$$

From a practical point of view, the increase in length should be kept as small as possible, and the expression for the length-factor shows that $C \cdot Y_s$ should be large — thus Y_S must be large. Because $Y_S = Y_I$, this means that the input admittance of the amplifier must be large, or, in other words, an amplifier with low input impedance is required. At the same time, however, it is required that i_T should be as small as possible. In a transistor amplifier these two requirements are not independent of each other. In general terms, the noise is reduced by decreasing the emitter current, which, in turn, increases the input impedance. This complicates the design of the input amplifier. It was found, however, that a common base amplifier stage could be of some advantage in this respect, and the system to be described next is based on this technique.

The block diagram of the complete amplifying chain is shown in Fig. 17. As seen, a transformer couples the electrode system to the preamplifier. Originally, it was intended to avoid a transformer, but initial tests showed that it was impossible to balance the stray currents between the single electrodes and the zero-potential line of the amplifier. The direct connection between the electrode system and the amplifier also restricted the length of the cable between the two parts of the equipment. These difficulties were therefore avoided by introducing the transformer. A cable of 800 m. between the transformer and the amplifier was used without any deterioration in the characteristics of the set-up.

The transformer is wound on a toroidal core of high permeability material having an external diameter of 14 cm, an internal diameter of 8 cm, a length of 3 cm and a lamination of 0.15 mm. The turns ratio of the transformer is 5, and the lower cut-off frequency is 0.2 cps. The transformed dipole impedance is 75 ohms, and,with a total cable resistance of 25 ohms, gives a total source impedance for the amplifier of 100 ohms. Fig. 17 shows that the first amplifier has a balanced input and that the cable is driven as a screened, balanced pair cable. This is a necessary precaution in order to reduce pick-up to a minimum. In a similar way, the transformer has balanced windings and is, furthermore, screened with a heavy, soft-iron box of 10 mm. wall thickness.

The amplifier chain consists of a balanced DC-feedback amplifier with a parallel stabilizing amplifier, a differential amplifier converting the balanced output of the preamplifier to an unbalanced signal, andl finally, a filter amplifier for the attenuation of 50 cps power-line interference. For completeness, Fig. 17 also shows a variable LP-HP filter, together with the modulator for tape recording to be described later.

The heart of the whole chain is the balanced DC-preamplifier, the circuit diagram of which is shown in Fig. 18. Its present design is a hybrid amplifier with a pair of valves, V_1 and V_2, following the common base stage, consisting of Q_1 and Q_2. The reason for this hybrid construction is that the high output impedance of the common base amplifier requires a high input impedance in the following stage. At the time of construction, no reliable field-effect transistors were available, but in future these transistors should be used.

The common base input stage uses selected pairs of type 2N2484 transistors, operated with equal base-emitter voltages for maximum stability. This technique is similar to the one described by Hoffart and Thornton (Ref. 13), but their paper

was not known by the EM Group when constructing the present amplifier. The stability of the circuit is supported by the very low DC-resistance that the cable and transformer present to the input of the first stage.

The amplification is determined by the source and feedback resistances, and is equal to 2 Rp/Rs. Although the amplifier is basically a DC-amplifier the lowest frequency of interest for the present project is, however, 1 cps, and the DC stabiliser, shown in Fig. 17, is used to stabilise the operating conditions and to introduce a well-defined cut-off. In the present adjustment, the lowest 3 db frequency is 0.2 cps and the slope is 6 db/octave.

The filter amplifier attenuates the 50 cps power line interference by 46 db and has a frequency characteristic with 3 db points at 33 and 85 cps. The variable band-pass filter following the amplifier is a tunable Allison 256, LC-filter, which has a slope of 28 db/octave. In general, this filter is set at 1 and 32 cps.

The characteristics of the amplifier in operating condition are as follows:

Bandwidth: without DC stabiliser:	0 - 200 cps
with " "	0.2 - 200 cps
Amplification: with R_S = 100 ohm:	6,600
Dynamic Range:	90 db
Feedback:	34 db
Input impedance at points 1 - 1:	$\approx$ 1 ohm
Ouput impedance at points 2 - 2:	$\approx$ 1,000 ohm

Noise characteristics with R_s = 100 ohm:

Noise factor in range 3 - 6 cps:	10.4 db
" " " " 6 -12 "	9.5 db
" " " " 12- 24 "	8.6 db

Including the transformer, and with a 3 ohm resistance as a substitute for the electrode system, the amplifier noise corresponds to $1.5 - 2.4 \times 10^{-10}$ $vpm_{(rms)}$ per $\sqrt{cps}$ in the frequency band 1 - 32 cps.

3.3 Recording Systems

An easy and widely used method for recording and displaying ELF noise has been paper recording. The recordings are generally used for waveform studies, investigation of number and time of occurrence of certain types of characteristic waveforms, or similar purposes. The rectified and smoothed signal is often displayed as well, in order to identify variations in the average level.

Other recording methods are now available and paper recorders are run as monitors in parallel with tape recorders, or the tape-recorded signals are played back to a paper recorder for visual inspection and selection of interesting parts of the recording.

During the earlier phases of the research programme, no battery-operated tape-recorder suitable for long term data acquisition in the 1-100 cps range was available. It was thus necessary for the EM Group to develop a recording system.

3.3.1 Direct Recording on a Low-Speed Tape-Recorder

Two basic ideas directed the development of the recording system. Firstly, it was desirable to have a battery-operated instrument suitable for long-term,

unattended data acquisition at the station on Tino. Secondly, the analysis of the recorded signal was to be made with instruments already available at the Centre for acoustic studies. These two requirements resulted in a low-speed tape-recorder compatible with the AMPEX FR600 tape machine used for playback. The final instrument has been described in detail by Marthins (Ref. 14).

Playback was at a speed of either 62.5 or 125 times the recording speed, which placed the signal within the audio-frequency range for spectrum analysis. The equipment used for this analysis does not require a description here.

3.3.2 An AM Modulator/Demodulator for a Commercial Tape-Recorder

The experience gained with the above-mentioned direct recording system exposed some of the drawbacks of this method. Firstly, it was not possible to check the recording on the spot, which means that failures would first be recognized only during the analysis. Secondly, it is very difficult to select special parts of the recording for detailed analysis because of the time-compression caused by the speed-up. In addition, it was desired to place a number of recording stations at widely separated points without direct communication between the stations and, as it was decided to place a tape-recorder at each station, the low-speed tape-recorder described above was found to be too expensive.

To overcome these drawbacks, a new system was developed based on a semi-professional UHER 4000-S tape-recorder that appeared on the market during the spring of 1963. This can be operated from various power sources, including a 6 v car battery; four speeds are available and the wow is reasonably low at the higher speeds.

The manufacturer announced that the UHER 4000-S tape-recorder would be the forerunner of a two-track model with similar characteristics. As the requirements of the complete recording system could thus be fulfilled with a single-

channel modulation system, it was decided to utilize amplitude modulation.

The block diagram of the AM modulator is shown in Fig. 19. The signal — the level of which is adjusted by the attenuator — is amplified and converted into a symmetrical push-pull signal. This then modulates a 2 kc carrier in a symmetric ring-modulator consisting of four transistors, and the resulting AM signal, without carrier, is recorded on the tape. In order to transmit the exact carrier frequency, a series of pulses with 2 kc repetition rate, but with suppressed fundamental-frequency component, are superimposed on the signal to be recorded. These pulses are later used for the generation of a carrier that demodulates the signal.

The complete circuit diagram of the modulator is shown in Fig. 20. The carrier oscillator is a multivibrator, consisting of Q8 and Q9 followed by a limiter (Q10, Q11), which produces a symmetrical square-wave at 2 kc for the switching of the ring modulator. The modulator consists of Q16, Q17, Q18 and Q19. The low frequency signal is amplified by Q1, Q2, Q3 and Q4 and converted to a symmetric signal by Q14 and Q15. The modulated signal is amplified in the tuned amplifier built around Q20. Pulses with a repetition frequency of 2 kc are generated by differentiating the 2 kc square wave and are added to the modulated signal after the fundamental frequency has been removed by Q13.

The demodulator, a block diagram of which is shown in Fig. 21, consists of a separator, a carrier frequency generator and a synchronous detector. Fig. 22 gives a complete circuit diagram of the demodulator. The upper channel contains an amplifier, which, after the rejection of the super-imposed pulses in the first stage, produces a symmetric signal that is applied to two of the inputs of the 4-transistor ring-modulator consisting of Q6, Q7, Q8, and Q9.

In the lower channel, the modulator signal is rejected in the first stage Q20. The remaining pulses are shaped in a pulse-shaper consisting of Q16...Q19, whereas the remaining part of the channel generates a symmetric square-wave which is applied to the other two inputs of the ring-modulator.

One of the advantages of this modulating system was its fairly high dynamic range, which, including the tape-recorder, was 50 db.

Unfortunately, it turned out that the two-track model of the tape recorder would not be available within the time required. Since the AM system was not suitable for multiplexing on to one channel, a fairly simple FM multiplex system with two channels was developed, as described below.

3.3.3 An FM Multiplex Modulator/Demodulator for a Commercial Tape-Recorder

The block diagram of a two-channel FM modulator is shown in Fig. 23. Each channel consists of a pulse-frequency modulator (PFM), a flip-flop (FF), and a low pass filter. The pulse-repetition frequency of the PFM depends on the instantaneous voltage of the input. The pulses trigger the flip-flop and in this way generate a square wave at half the frequency of the PFM. The filter removes the harmonics of this square wave and is designed for highest attenuation in the frequency band occupied by the second channel. Apart from the components that determine the frequency, the two channels are equivalent.

A complete circuit diagram of the modulator is shown in Fig. 25. (As the two channels are equivalent, only one channel is shown on the diagram). A circuit described by Schwartz (Ref. 15) has been utilised for converting the low-frequency modulating signal into pulses with repetition frequency proportional to the amplitude of the low frequency signal. In this circuit, the condenser C is

charged with a constant current proportional to the input voltage. A short pulse is generated by the firing of the unijunction transistor Q2. This pulse triggers the flip-flop, which consists of a Philips FF1 building block. The rest of the circuitry is straightforward. To avoid the usual difficulties when the frequency goes outside the passband of the low-pass filter, the input signal is limited by a simple diode clipper. The proper recording level is adjusted on the tape-recorder itself.

In the demodulator, the block diagram of which is shown in Fig. 24, the two channels are separated by corresponding low-pass and high-pass filters. After amplification, a pulse shaper (PS1) generates a square wave, the leading edge of which triggers a one shot multivibrator (OS1). The output from OS1 consists of pulses of fixed area with a repetition frequency corresponding to the modulating signal. The average value of the output of OS1 is thus proportional to the instantaneous value of the low frequency signal.

The complete circuit diagram is shown in Fig. 26. Use is made of standard building blocks for the pulse shaper and one shot multivibrator. The output amplifier for each channel has two outputs with 180^{o} phase difference, which provides an easy method of obtaining the difference between the two channels.

Since the lowest frequency in the range of interest is 1 cps, no provision is made for a frequency response down to DC. On the contrary, a number of difficulties inherent in FM-systems with DC response could be avoided. Slow drifting of the frequency does not present any problem, and the requirements of the tape-recorder are not severe. Basically, the modulator/demodulator can be used at any tape-speed provided that the frequency response of the tape-recorder is adequate. It has to be kept in mind, however, that most commercial tape-recorders have the lowest wow and flutter at the higher tape speeds. With the

UHER 4000-S, speeds of 7 1/2 in/sec and 3 3/4 in/sec have been used with satisfactory results.

Some characteristic data of the modulator/demodulator are :

Frequency response:	- 3 db at 0.2 and 200 cps
For the range between 1 and 32 cps the following performance was obtained:	
Phase difference between the two channels:	$\Delta\varphi \leq 3^{\circ}$
Max. input signal at which the distortion is less than 1%:	$v_{imax} = 0.7\ v_{rms}$
Output signal corresponding to v_{imax}:	$v_{omax} = 0.35\ v_{rms}$
Noise level at output for input terminated in 600 Ω :	$v_N \approx 0.8\ m\ v_{rms}$
Crosstalk attenuation between channels:	> 50 db

All the above data were measured without the tape-recorder.

4. PROCESSING AND ANALYSIS OF EM BACKGROUND NOISE DATA IN THE ELF RANGE

The processing of the recorded ELF noise depends, as usual, on the information required and the way in which it should be displayed. In the past, paper recordings have been the most common method, and visual inspection was generally the only system of processing used. An experienced observer is able to distinguish between several characteristic waveforms and will generally classify them according to his own rules. This technique has been utilised widely and has revealed information on the frequency of occurrence of certain phenomena, coherency between commencements, etc. Naturally, more information can be obtained if each record is processed in greater detail, and some of the more useful techniques will be described below.

4.1 Waveform Display

Even if a waveform display only yields limited information it is still very useful, and normally no detailed analysis is made before a paper recording has been inspected visually. The main purpose of such an inspection is generally to distinguish between those parts of the recordings that are obviously of no interest and those which should be analysed further. If paper recordings from more than one station are lined up side by side, they immediately show certain signals that appear simultaneously at both stations. Fig. 27 shows an example of two such recordings. The sample shown is only about 3 sec long and compares measurements taken simultaneously on Tino and on the west coast of Canada. Both measurements were made with identical loop equipment for all three orthogonal components, but only the x-components are shown here. The original signal was filtered with an 8 - 25 cps filter before display.

The "visual correlator", however, has a very limited range. As demonstrated by Madden (Ref. 2), the lower limit of visual correlation corresponds to a correlation factor of about 0.95. Signal recordings that look completely uncorrelated to the visual correlator may actually show a correlation factor of about 0.8. It is thus reasonable to expect that more information can be extracted by correlation techniques or power-spectrum analysis — two methods which basically extract the same amount of information from a given sample.

4.2 Power Spectrum Analysis

4.2.1 General Problems

The representation in the frequency domain of time-varying phenomena is a very common technique, and is often used for the detection of special frequency components in a mixed signal. The power spectrum analysis is thus useful in the case of background noise, especially because it is possible to estimate the accuracy of the measurement. As a matter of fact, no more than an estimate of the true power spectrum can be made from a finite sample of the background noise, but the parameters of the measurement permit the investigator to calculate how good the estimate is. Details of the power spectrum analysis will not be given here. Blackman and Tukey (Ref. 16) have given a very thorough treatment of the subject in general, and Zukerman (Ref. 17) has applied the theory to sweeping spectrum-analysers.

The main problem in analysing the background noise is normally that of finding the proper combinations between the resolution, the stability of the measurement and the sample length. The relations between these three parameters have been plotted in Fig. 28. The vertical scale is the dimensionless product, $T_n W_e$ of the length of the sample T_n and the effective filter bandwidth W_e. (This

product is equal to half the degrees of freedom, k). The parameter of the curves is the fraction of distribution, and the horizontal scale indicates the interval within which the true value would be found with the given distribution. For example, with $T_n W_e = 10$, 80% of the distribution will fall within an interval of 3.5 db. The distribution is not symmetrical and, in this example and assuming a single sweep, there are eight chances out of ten that the true value is within −1.5 db and +2.0 db of the observed value. For values of $T_n W_e$ greater than about 25, the distribution becomes symmetrical and the parameters of the curve can be interpreted as probabilities. Fig. 29 has been constructed for the lower values of $T_n W_e$. The curves indicate the upper and lower limits of the ratio between true and measured value for various probabilities.

With the help of these two sets of curves it is possible to plan the measurements for given parameters, or to calculate the stability of a given set of sample length and bandwidth. The curves also show how "expensive" it is to make good estimates. If, for example, an interval spread of 1 db ($\pm$ 0.5 db) is required with a probability of 0.98, then $T_n W_e$ must be 440. Suppose that the required resolution is 0.2 cps, then T_n must be about 36 min.

It is clear from the above remarks that the estimate of power spectra needs careful planning. This is especially the case when there are limits on the signal that has to be analysed. Figures 28 and 29 have been computed on the basis of stationary Gaussian processes. It is furthermore assumed that the spectrum does not vary drastically within the bandwidth W_e. If the spectrum contains lines, one has to make corrections to the true degree of freedom before estimating the accuracy of the measurement. Both references mentioned above give details for the case of spectrum variations within W_e.

Another limit is equally important — that of time. The curves are calculated for a single sweep of the spectrum analyser. The required sample length T_n may be longer than the available sample, or it may turn out that the signal cannot be considered as stationary for extended periods of time. As mentioned in Chapter 1, the level of the background noise due to micropulsations follows a diurnal pattern. The same seems to be true for the frequencies in the Schumann modes. These variations restrict the length of the sample within which the process can be considered as stationary. It would, however, be safe to assume 15 min as the maximum. Balser and Wagner (Ref. 18) used 12 mins for the estimate of the power in the resistance peaks. Their bandwidth was 1/3 cps, which gives an interval spread of 1 db.

Digital calculations of the power-spectrum permit the maximum utilisation of the recorded data. The analogue spectrum analyser has the advantages of being flexible and easier to transport. The accuracy of the spectrum estimates is lower, however, and has to be taken into account when interpreting results.

A brief description of the analogue analyser used is given below.

4.2.2 Spectrum Analysis with the ISAC Statistical Analogue Computer

The statistical analogue computer ISAC* is a tape-loop machine suitable for auto- and cross-correlations, power and amplitude spectrum analysis, and amplitude distribution function. In the present section only the power spectrum part and its use will be described.

---

*ISAC (Instrument for Statistical Analogue Computations), developed by the Engineering Res. Foundation of the Technical University of Norway. Produced by NORATOM A/S, Oslo, Norway.

The block diagram of this part of the instrument is shown in Fig. 30. The original signal is frequency-modulated and recorded on a magnetic-tape loop. For analysis, the recorded signal is played back through a demodulator and passed through a narrow bandpass filter after heterodyning with a sweeping frequency in the mixer. The output of the filter is squared and smoothed by a low-pass filter and is then displayed as Y on an X-Y recorder. The X-position of the pen is controlled by the sweep generator, the total spectrum being recorded by a single sweep.

The instrument covers the frequency range of 0 - 200 cps in the playback, and the fixed band-pass filter has an effective bandwidth of 1.5 cps at its highest speed. The signal can be recorded at different lower speeds by a speed selector, which also changes the modulator accordintly. If, for example, the recording is made at 1/8 of maximum speed, the highest frequency will be $200/8 = 25$ cps. The effective bandwidth of the filter will correspondingly be $1.5/8 \approx 0.2$ cps. The sweep rate and the time constant of the low-pass filter can be varied according to the problem on hand.

The accuracy of the estimate is set by the design of the analysing section and the choice of the tape-loop length. The effective bandwidth of the filter is 1.5 cps, and two tape-loops of 5 and 15 sec each are available. This gives a $T_n W_e$ product of 7.5 and 22.5, which means that, with a probability of 0.90, the true value will fall within the following ranges around the measured value:

5 sec. loop	- 2.2 db	to	+ 3.2 db
15 " "	- 1.3 db	to	+ 1.6 db

Recording at lower tape speeds does not change the product of T_n and W_e, because the analysis itself is always made at maximum speed. If a higher

accuracy is needed, then the average of a number of pieces can be taken. A general relation between the probability, the interval spread, the number of pieces and the resolution has been given by Blackman and Tukey (Ref. 16) in the case where the spectrum is reasonably flat.

$$(\text{No. of pieces}) = \frac{\frac{1}{2} + \frac{200}{(0.90 \text{ range in db})^2}}{(\text{length of each piece})(\text{resolution in cps}) - \frac{1}{3}} \qquad \text{(Eq. 49)}$$

For the ISAC, using the 15 sec. loop and 1.5 cps resolution, this gives:

$$(\text{No. of pieces}) \approx \frac{9}{(0.90 \text{ range in db})^2} \qquad \text{(Eq. 50)}$$

It is seen that a 3 db range corresponds to one piece, which is in accordance with the interval given above.

It is now possible to estimate the accuracy of the measurement with the ISAC when a maximum sample length of 15 min is used. The frequency range of interest starts at 1 cps and, if the lowest octave from 1 - 2 cps has to be resolved into five frequency bands, this corresponds to a bandwidth of 0.2 cps. This is obtained if the signal is recorded at 1/8 of maximum speed. The length in real time of the long loop is then 8 x 15 = 120 sec. The total sample length can thus be split into 6 pieces, which, according to Eq. 50, gives an interval spread of 1.2 db. The maximum frequency resolved is 25 cps.

A few remarks should be made about the sweep rate and the time-constant of the low-pass filter, both of which can be selected independently on the ISAC. As was mentioned, the $T_n W_e$ product was set by the playback section, giving either 7.5 or 22.5 according to the loop used. For a reasonably flat spectrum the sweep rate should then be 0.3 and 0.1 cps respectively, and in this case no correction is needed for the apparent increase in bandwidth and decrease in response. If, however, the spectrum contains sharp resonance lines, a correction has to be made, as shown by Zuckerman (Ref. 17). This problem can be overcome by calibrating the instrument with signals of known power and frequency.

The same calibration procedure can be used to determine the influence of the time constant of the low-pass filter. Ideally, the low-pass filter should have a weighting function that is constant for time delays between zero and T_n and is otherwise zero. This cannot be obtained in an analogue system, and, as a first approximation, a cut-off frequency of 1/3 of the reciprocal of the integration time can be used. For the two sample lengths of 5 and 15 sec, this would correspond to cut-off frequencies of 0.066 and 0.022 cps respectively. The problem of the long time-constants is overcome by using a loop, so that the original signal becomes strictly periodic at a period corresponding to the inverse of the sample length. During playback the instrument is adjusted in such a way that the zero-frequency component is nulled. The lowest frequency present in the output then becomes the one corresponding to the revolution of the loop. The low-pass filter can then be designed in such a way that the power content of that frequency is sufficiently attenuated.

In the ISAC a number of time-constants can be chosen, and by proper selection of sweep-rate and time-constant it is possible to obtain a smooth estimate of the power spectrum showing a reasonable number of details. The best combination of these is usually found by a quick trial run that gives a rather rough estimate of

the spectrum. This trial run also shows if the spectrum is flat enough to make use of the stability calculations. The accuracy of the instrument has been found adequate for general purposes. A digital analysis is, however, to be preferred in those cases where the maximum amount of information has to be extracted from a given sample.

All spectra recorded and analysed with the same adjustments of the instrument can be compared directly, and such a comparison can reveal interesting information. Often, however, an absolute measure of the rms level is required, and in that case a calibration has to be performed. Normally, such a calibration embraces the total measuring equipment, including all amplifiers, filters, etc., and is made by injecting a known signal at the input. The power spectrum of this is then measured with the same settings for sweep-rate and time-constant. Since the X-axis is calibrated in cps and the Y-axis gives the power density in v_{rms}^2/cps, a graphical integration with a planimeter gives the calibration factor in v_{rms}^2/cm^2. From this, the rms level per unit bandwidth can be calculated at any given frequency.

A few examples of power spectra of the EM background noise are given in Section 6.

4.3 Correlation Techniques

4.3.1 Procedures

As mentioned before, power spectrum analysis and auto-correlation extract the same amount of information from a given sample, provided the processing is optimized. Generally, there is no need to calculate the auto-correlation function if the power spectrum can be obtained directly. In a digital system, however, the

general procedure is to compute the auto-correlation function and to obtain the power spectrum by a Fourier-transform. There may, however, be other reasons for computing correlation functions. An example of such a case will be given in the next section.

In practice, the computation of the correlation functions is also made with the ISAC. No details will be given about the technical part of calculations. As was the case with the power spectrum, the signal is recorded on tape-loops, and a movable head provides the required time delays, τ , in steps of 0.8 or 3.2 ms in playback time. In this way either 400 or 100 points of the correlation function can be computed. The stability of the correlation function estimate is subject to the limitations set by the length of the loops and the time lag, and will not be treated here. With integration times of 4 and 14 sec respectively, the number of degrees of freedom is higher than during power spectrum analysis, and the estimates of the correlation function are thus more stable than the power spectrum estimates. The output of the correlator is displayed as points on the X-Y recorder. The instrument has three channels, and it is thus possible to perform estimates of both auto- and cross-correlation functions. This facility is rather useful, even if the interpretation of correlation functions is generally more difficult than the equivalent display in the frequency domain.

4.3.2 Separation of Noise Sources by Correlation

The spatial coherency of the background noise, when measured in a "clean geometry", can be used for the separation of noise sources. The term "clean geometry" refers here to conditions where the measurement is made far from coastlines, over deep water and within distances that are small compared with wavelengths in air. Conversely, the degree of coherence can be used to characterise the influence of the bottom, coastlines, etc.

In both cases, two separate channels are required. Suppose that the two channels have technically equal electrode systems aligned in parallel, and that the separation between the two systems is at least 2 skin-depths. For the lowest frequency of interest, 1 cps, this would be a separation of about 0.5 km. The two amplifier channels are assumed to have equal amplification, frequency and phase characteristics. Both channels have, however, separate noise sources, and the outputs of the channels can be expressed as a function of time in the following ways.

The output from Channel 1 is:

$$f_1(t) = S_c(t) + S_u(t) + N_1(t) \qquad \text{(Eq. 51)}$$

where $S_c(t)$ represents the coherent part of the background noise, $S_u(t)$ represents the incoherent part, and $N_1(t) = E_1(t) + A_1(t)$ represents the noise due to the electrodes and amplifier. It is assumed that the noise sources do not contain periodic components and that their average is zero. The output from Channel 2 can be written in a similar way:

$$f_2(t) = S_c(t) + N_2(t) \qquad \text{(Eq. 52)}$$

According to the above definition, $S_c(t)$ in Channel 2 is the same as in Channel 1. All uncorrelated parts of the background noise have been concentrated in the term $S_u(t)$ in Channel 1. This means that Channel 2 is used as a reference for Channel 1. It is clear that if there is complete coherence, $S_u(t)$ is zero. $N_2(t) = E_2(t) + A_2(t)$ has the same meaning as above but is different from $N_1(t)$.

The auto-correlation function for the output of Channel 1 is:

$$\varphi_{11}(\tau) = \overline{\left[S_c(t) + S_u(t) + N_1(t)\right] \quad \left[S_c(t-\tau) + S_u(t-\tau) + N_1(t-\tau)\right]}$$

(Eq. 53)

$$\varphi_{11}(\tau) = \varphi_{SS_c}(\tau) + \varphi_{SS_u}(\tau) + \varphi_{NN_1}(\tau)$$

All other terms cancel, because the sources are incoherent. Similarly, the auto-correlation function for the second channel is:

$$\varphi_{22}(\tau) = \varphi_{SS_c}(\tau) + \varphi_{NN_2}(\tau) \qquad \text{(Eq. 54)}$$

The cross-correlation between the two channels is computed as:

$$\varphi_{12}(\tau) = \overline{\left[S_c(t) + S_u(t) + N_1(t)\right] \quad \left[S_c(t-\tau) + N_2(t-\tau)\right]}$$

$$\varphi_{12}(\tau) = \varphi_{SS_c}(\tau) \qquad \text{(Eq. 55)}$$

All other products cancel out, because the sources are incoherent. The cross-correlation between the channels thus gives the auto-correlation function of the coherent part of the background noise.

The value of the auto-correlation function at $\tau = 0$ represents the square of the rms value of the signal. Applying this to Eq. 53, 54 and 55 gives:

$$f'^{2}_{1} = S_c^2 + S_u^2 + N_1^2$$

$$f'^{2}_{2} = S_c^2 + N_2^2 \qquad \text{(Eq. 56)}$$

$$f'^{2}_{12} = S_c^2$$

where f', S_c, S_u and N represent the rms values of the sources concerned.

If there is complete coherence in the background noise, then $S_u(t)$ is zero, and the three expressions permit the separation of $N_1(t)$ and $N_2(t)$ from the wanted signal $S_c(t)$. When the two noises have been determined by an experiment that eliminates S_u, the expressions can be used to determine the degree of coherence under other circumstances. A special case is the one where the two systems are not parallel and thus measure slightly different components of the field. The degree of coherence is in this case a measure of the alignment of the electrode systems.

A number of practical problems arise when the above-mentioned scheme is put into practice. One problem — that of alignment — has already been mentioned. When using a floating platform at sea the relative position can only be maintained for a certain period of time. The problem could eventually be solved by using two electrode systems, perpendicular to each other, at each place. The actual background noise vector could then be computed by taking the square root of the sum of the squares of the voltages from each pair, and computing the correlation functions of the output. This method has not been put into practice.

Another problem is the computation of the correlation functions themselves. In the above theoretical treatment, an infinite time of observation (or integration) was assumed. Since the signal is only present as a stationary process during a limited time, all correlation functions have to be replaced by their respective estimates. This means that the noise sources are not cancelled completely, and this limits the accuracy of the measurement. Thus it is only possible to estimate the minimum value of the coherence.

In the above treatment it was assumed that the various noise sources did not contain any periodic component. Nothing, however, was assumed about the coherent part of the background noise, and in theory this measuring technique should also be applicable when the background noise contains a periodic component. This technique was tried in a qualitative test, the result of which is shown in Figs. 31 and 32. There is a striking similarity between the auto-correlation and cross-correlation estimates. In all three cases there is a periodic component besides the random component. The estimates were made on the basis of a two-minute sample band limited at 4 cps and 32 cps. It is seen that the periodic component has a period of τ = 128 ms, corresponding to the first mode of the earth-ionosphere cavity resonance of approx. 7.8 cps. The two electrode systems were lined-up as accurately as possible at a distance of 250 m from each other, with water-depths of 150 and 75 m, respectively. The differences between the curves are shown in Fig. 30 and demonstrate the good coherence of the background noise signal. Although those differences are close to the noise level of the correlator itself, they seem to indicate that part of the periodic signal is uncorrelated in the two channels. The coherent part is, however, predominant and represents about 90% of the signal. The uncorrelated part can eventually be explained by a lack of parallelism between the electrode systems, and by the fact that the water-depth is about one skin-depth below one electrode system and about two skin-depths below the other. The reflection from

the sea-bed will thus be different in magnitude and phase for each of the two electrode systems.

In the test described, the background noise was much stronger than the noise of the electrodes and amplifiers,and, in the interpretation of the results, the latter noise sources were assumed to be zero. The test has shown that this technique can also be used in the case where the background noise contains periodic signals.

5. EXAMPLES OF EM BACKGROUND NOISE SPECTRA IN THE ELF RANGE

It will suffice to show a few examples of the background noise spectra. As mentioned in Chapter 1, the variations of frequencies above 5 cps follow a diurnal pattern, in which the ratio between the maximum and minimum power levels of the mode frequencies is about 1.5. The lowest part of the spectrum also depends on the geomagnetic activity.

The power spectrum estimate, shown in Fig. 33, is based on measurements made at sea in the La Spezia area, using the electrode system described in this report. The estimate is an average of six samples, each two minutes long in real time, and analyzed with a resolution of 0.2 cps. According to Eq. 49 the true level will be within 1.2 db of the measured one, with a probability of 0.90. It is seen that the field-strength in a 1 cps band, around the first mode of 7.5 cps, is about 1.2×10^{-9} v_{rms}/m. At 10 - 12 cps it is about 0.6×10^{-9} v_{rms}/m in a 1 cps band. The spectrum was limited at 4 cps because of excessive low-frequency noise, which was due to large movements of the electrode system. The mode frequencies indicated correspond well to those found in the literature.

Another power-spectrum is shown in Fig. 34. It represents the noise on the 1 - 25 cps band, as measured in a narrow Scottish loch. In comparison with Fig. 33 it is seen that the field-strengths are approximately four to six times higher in this case. This is explained by the position of the measuring site. The length of the sample and the resolution show that the interval spread is 3 db.

As a comparison of power spectrum estimates with auto-correlation and cross-correlation estimates, the same data that were analysed by the latter methods in Figs. 31 and 32 are shown in spectra form in Fig. 35. It is seen that the strong first-mode component is also evident here. The interval spread is 3 db, but the y-axis has not been calibrated because the test was a qualitative one only.

6. CONCLUSIONS

The present report has described the instrumentation developed by the EM Group for the measurement of the EM background noise from a floating platform at sea. These measurements, made in clean geometry, indicate noise levels somewhat lower than those measured on land. One probable explanation could be that the levels on land are subject to deep geological layers reflecting part of the energy. This phenomena has also been observed at sea when the water depth was limited.

Initial steps have been taken to study the spatial coherence of the background noise, and results of a preliminary test have been presented. The techniques used indicate that it would be possible to determine the influence of the sea-bed and coastlines on the background-noise fields.

The electrode system was selected on the basis of theoretical considerations of its behaviour during platform movements. It has proved to be a useful tool, and the experience gained permits an estimate of the behaviour of other detector systems for the same frequency range. The sensitivity of the system in its present state is sufficient for the measurement of noise levels in general. The design, however, is the result of a number of compromises and does not necessarily represent an optimum solution. The sensitivity, for example, could be increased, especially if the system is made to rest on the sea-bed, which is possible because the construction of the electrode system permits submergence to fairly great depths. A distance of 800 m. between the electrode system and the amplifier has been tried with good results, and eventually this distance may be increased still further if necessary. The use of two crossed systems is envisaged but has not yet been tried.

REFERENCES

1. L. Brock-Nannestad, "Bibliography of EM Phenomena with Special Reference to ELF (1-300 cps)", NATO SACLANTCEN, T.R. 25, October 1964.

2. T. Madden, "Instrumentation for Receiving EM Noise below 3,000 cps", article in "Natural EM Phenomena below 30 kcs", NATO Adv. Study Inst (D.F. Bleil), 1964.

3. J.E. Lokken, "Spectral, Cross-spectral and Bispectral Analysis of Low Frequency", article in "Natural EM Phenomena below 30 kcs", NATO Adv. Study Inst (D.F. Bleil), 1964.

4. R.M. Bozorth, "Ferromagnetism", van Nostrand Comp. Inc., 1951, Chapter 19.

5. H. Kaden, "Wirbelströme und Schirmung inder Nachrichtentechnik", Springer Verlag, 1959.

6. H. Rothe, W. Dahlke, T. Schubert, "Messungen der Konstanten des Funkelransehens", Telefunken Zeitung, Vol. 26, No. 99, March 1953, pp. 77-84.

7. J.R. Wait, "On the Relation Between Telluric Currents and the Earth's Magnetic Field", Geophysics, Vol. 19, No. 2, April 1954, p. 281.

8. R.C. Hansen, "Radiation and Reception with Buried and Submerged Antennas", IEEE Transactions on Antennas and Propagation, Vol. AP-11, No. 3, May 1963, pp. 207-216.

9. J.R. Wait, "The Magnetic Dipole Antenna Immersed in a Conducting Medium", Proc. IRE, Vol. 40, Oct. 1952.

10. J.R. Wait, "Insulated Loop Antenna Immersed in a Conducting Medium", J. Res. NBS, Vol. 59, 1957.

11. A. Silverstein, "The Deep Dip Electromagnetic Detector", U.S. Naval Ord. Lab. NOLTR 61-7, 1961.

12. P.J. Johnson, J.F. Orr, J.A. Zenel, "Measurements of Velocity-Induced Electrode Noise, Conducted from a Surface Boat on Long Island Sound", U.S.L. Technical Memo. No. 972-59-64, 15 April 1964, U.S. Navy Underwater Sound Lab., Proj. No. 1-113-02-00.

13. A.H. Hoffart, R.D. Thornton, "Limitations of Transistor DC Amplifiers", Proc. IEEE, Vol. 52, February 1964, pp. 179-184.

14. J. Marthins, "On the Recording of Low Frequency Signals on Magnetic Tape", SASWRC T.R. No. 6, 1962, and IRE Trans. on Instrumentation, Vol. I-11, No. 2, Sept. 1962.

15. J. Schwartz, "Unijunction Transistor Simplifies Voltage-Frequency Converter", Electronics, 25th Oct. 1963, p. 56.

16. R.B. Blackman, J.W. Tukey, "The Measurement of Power Spectra from the Point of View of Communication Engineering", Dover Publications, Inc., N.Y., 1959.

17. L.G. Zukerman, "Application of a Spectrum Analyser for Use With Random Functions", IRE Transactions on Instrumentation, Vol. I-10, No. 1, June 1961, pp. 37-43.

18. M. Balser, C.A. Wagner, "Diurnal Power Variations of the Earth-Ionosphere Cavity Modes and Their Relationship to World Wide Thunderstorm Activity", J. Geophys. Res., Vol. 67, No. 2, Feb. 1962, p. 619.

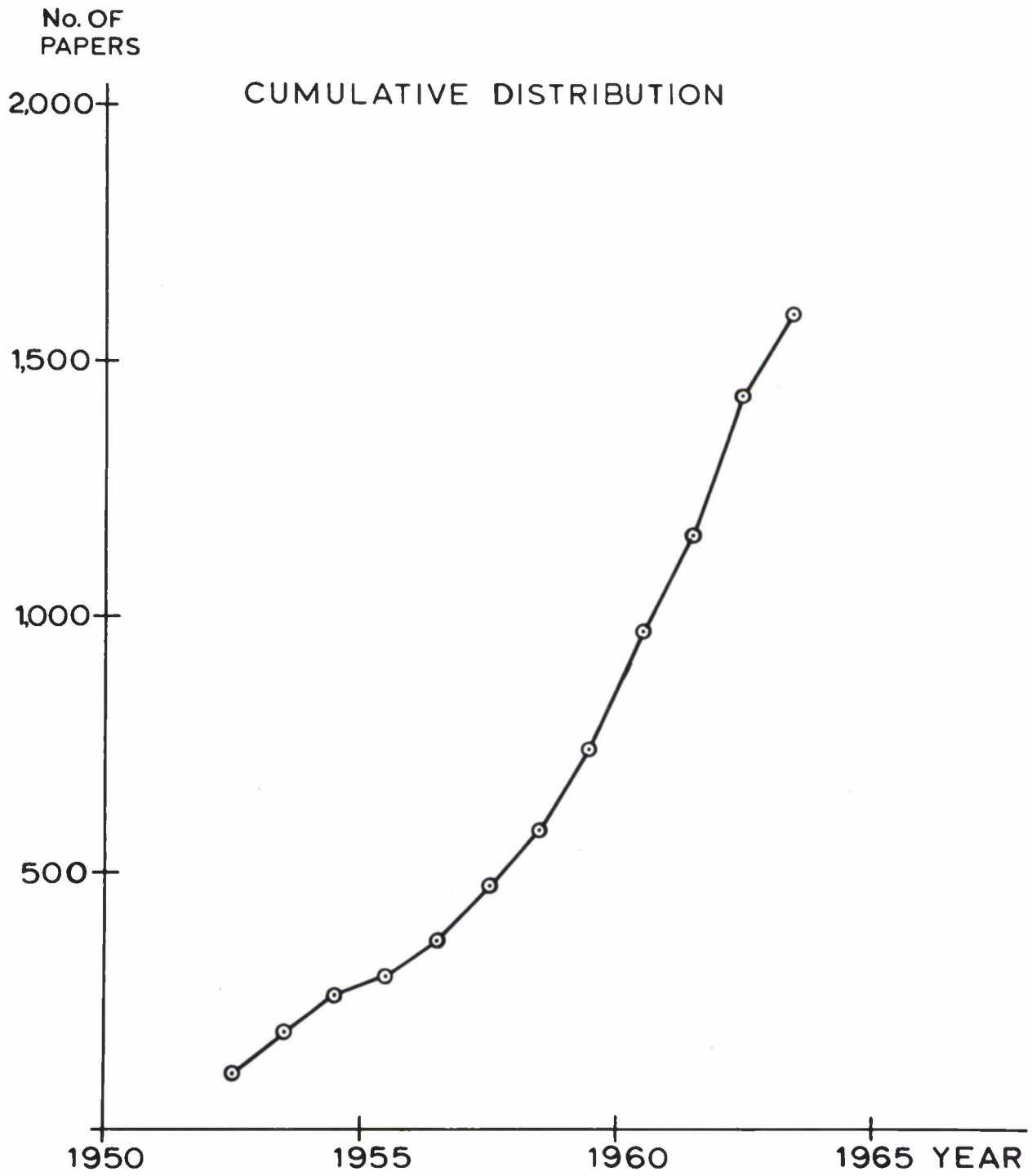

Fig. 1 Graph to show the rapid increase in the numbers of publications on EM phenomena in the frequency range 1 - 3, 000 cps between 1960 and 1964.

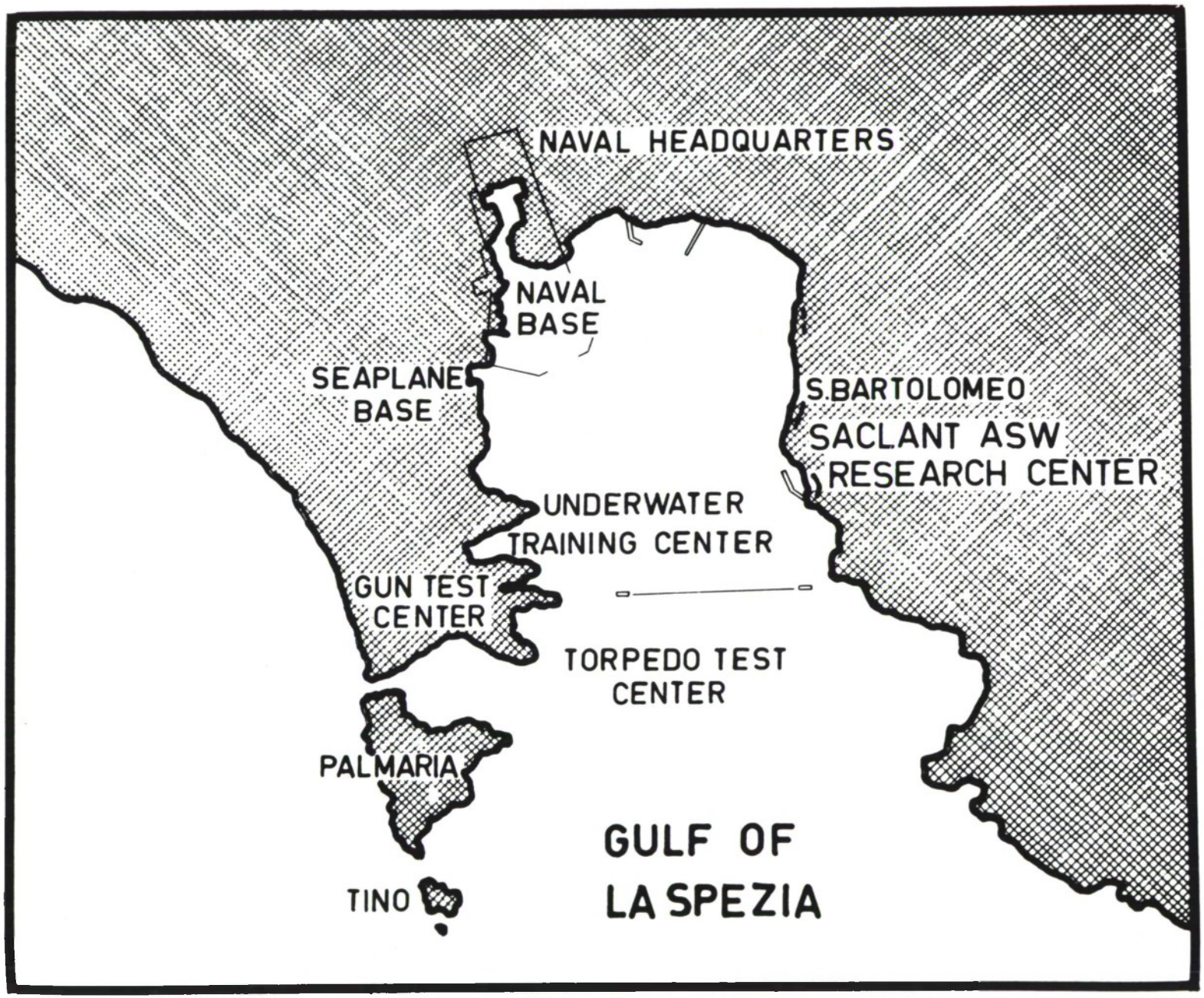

Fig. 2 The Gulf of La Spezia, showing the position of the Island of Tino on which measuring stations were erected.

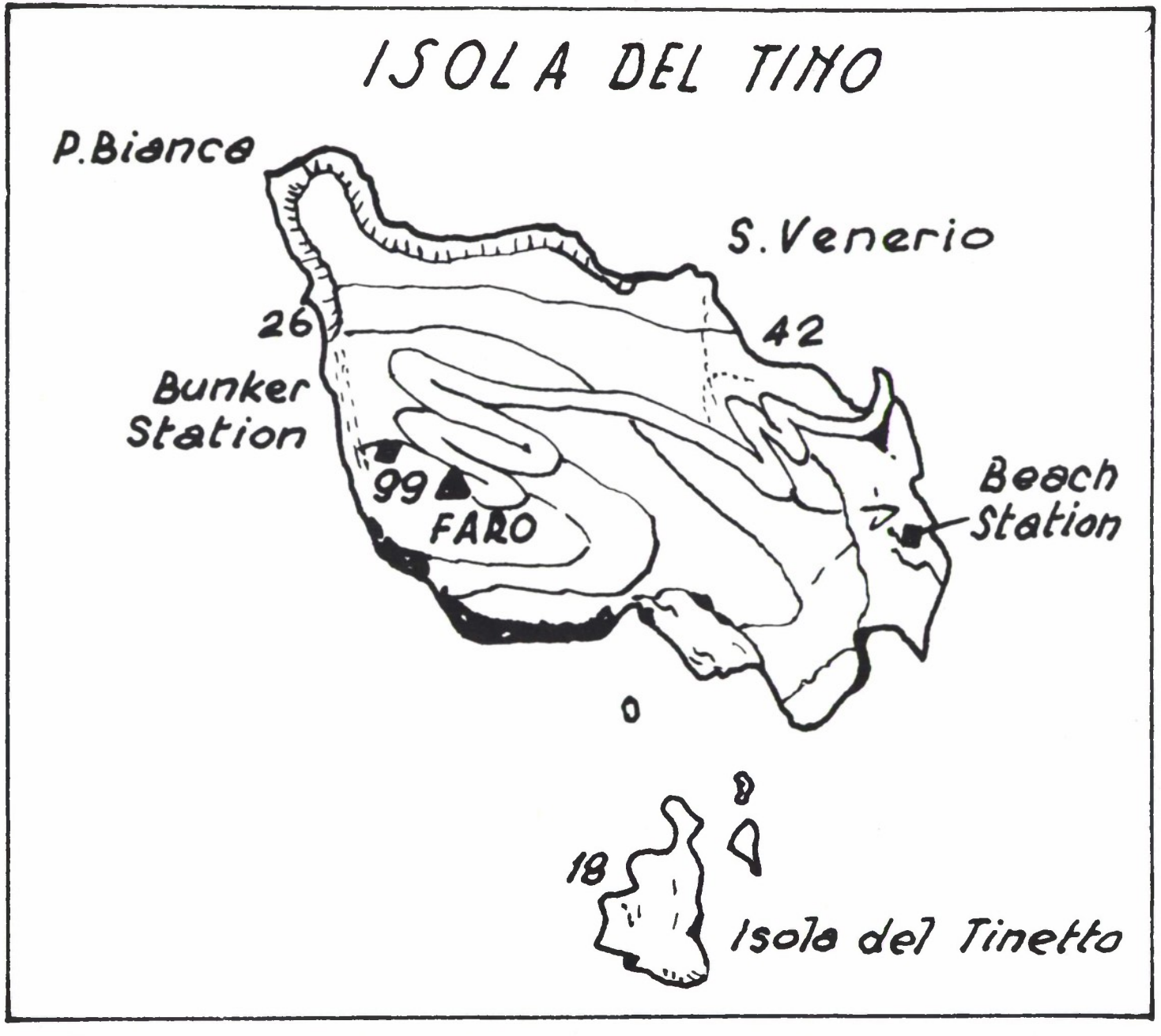

Fig. 3 The Island of Tino, showing the position of the two measuring stations.

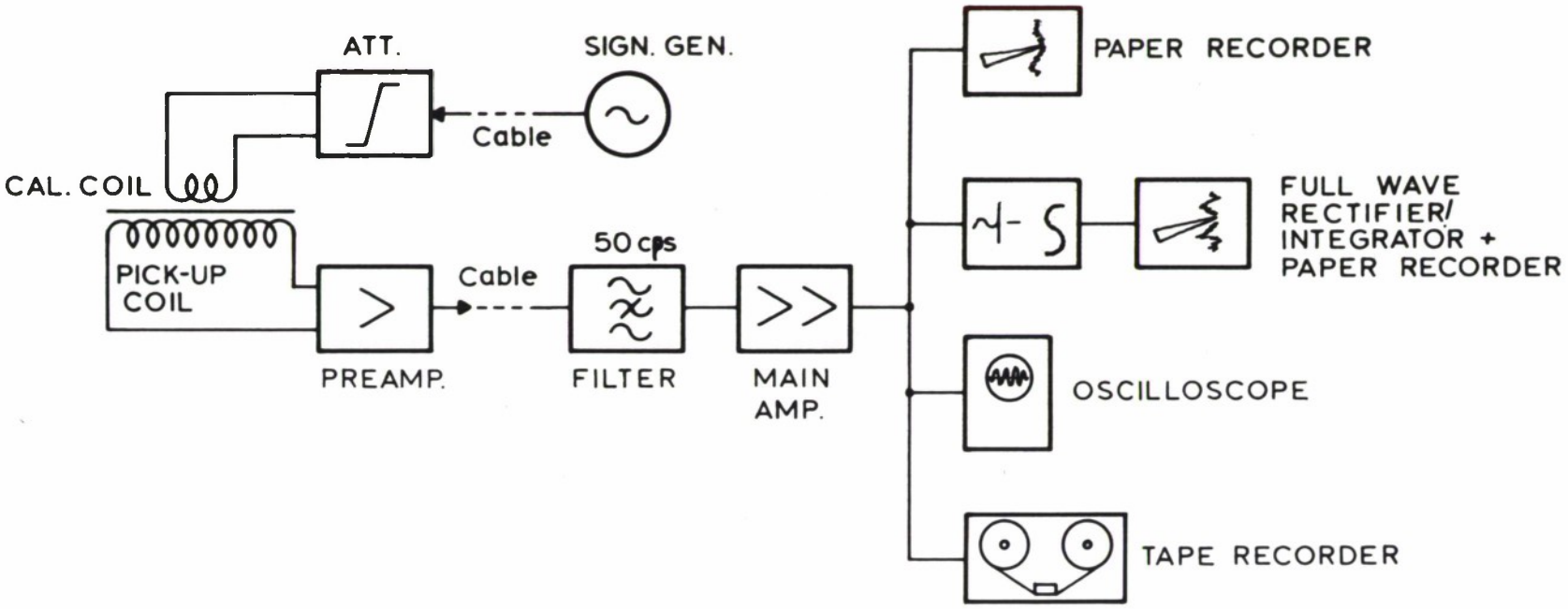

Fig. 4 Block diagram of the instrumentation for studies of the Horizontal Magnetic Component — the instrumentation for only one of the two channels is shown.

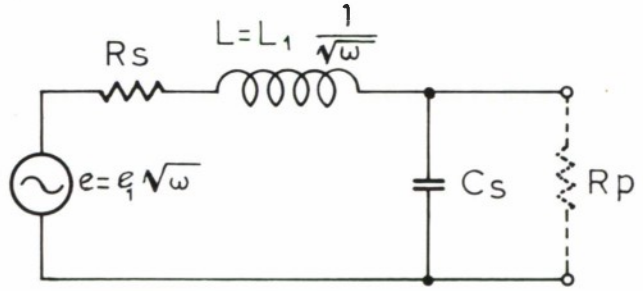

Fig. 5 Equivalent circuit for the Pick-up Coil.

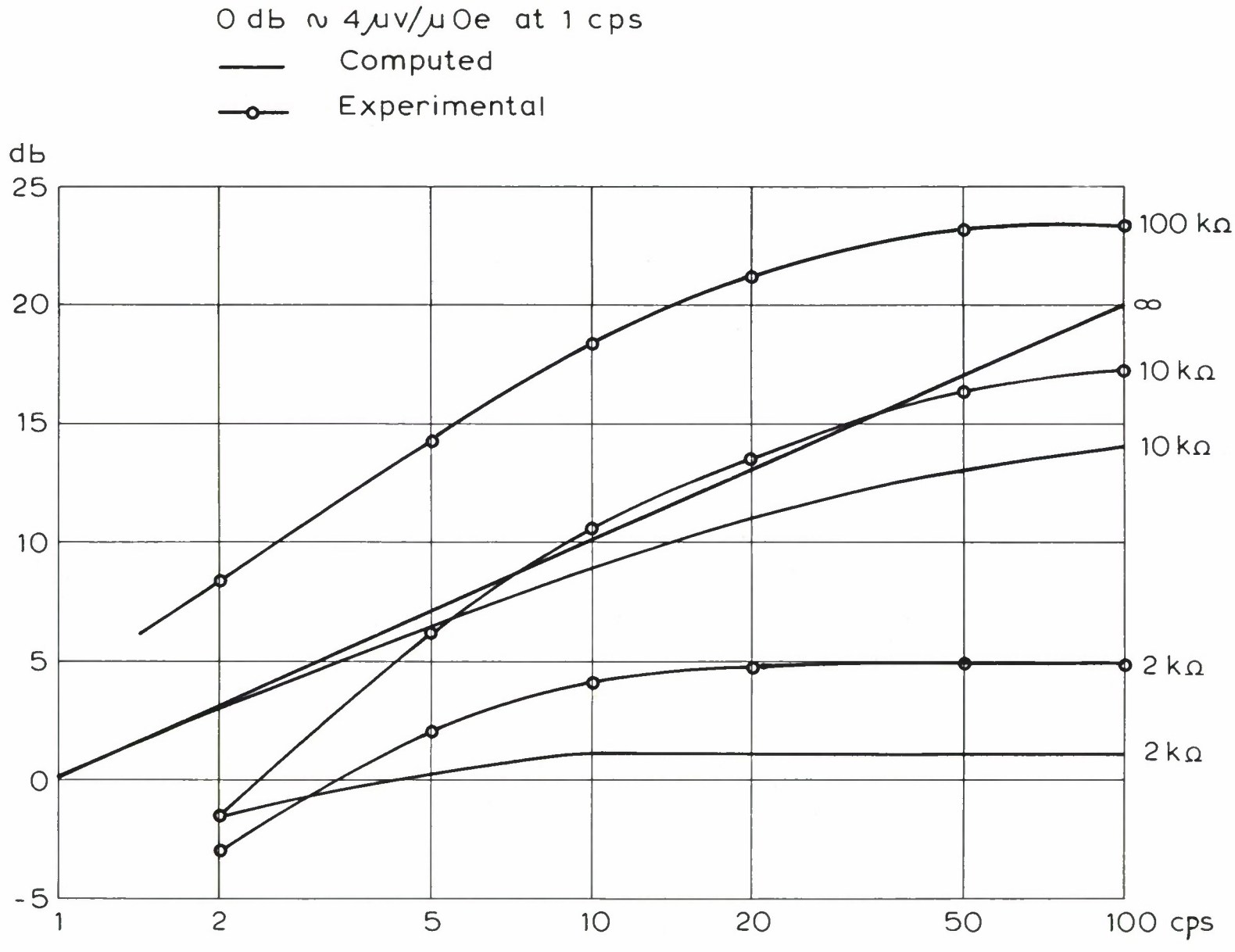

Fig. 6 Computed and measured frequency responses in the Pick-up Coil for three values of load resistance.

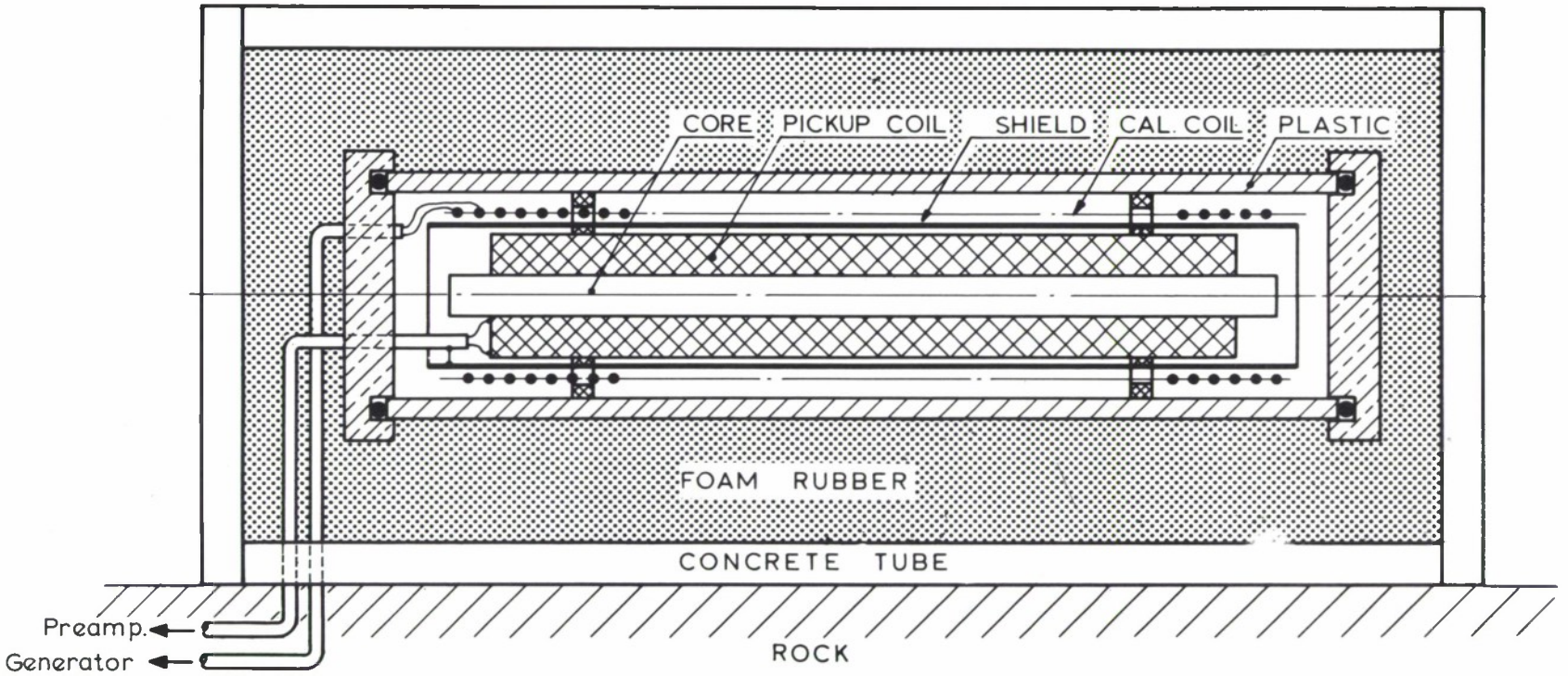

Fig. 7 Mechanical layout of the Pick-up Coil assembly and the Calibration Coil.

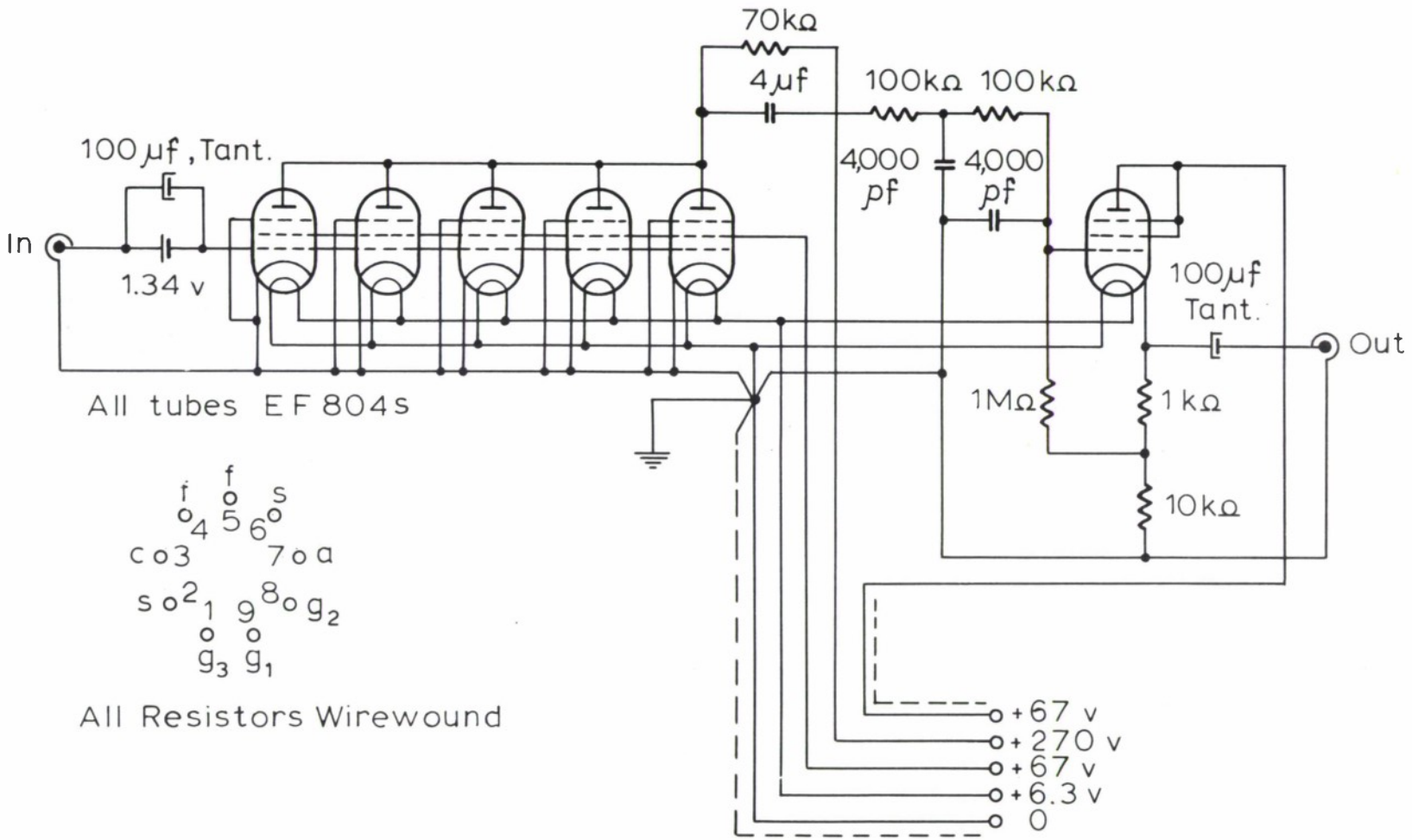

Fig. 8 Circuit diagram of the valve Preamplifier.

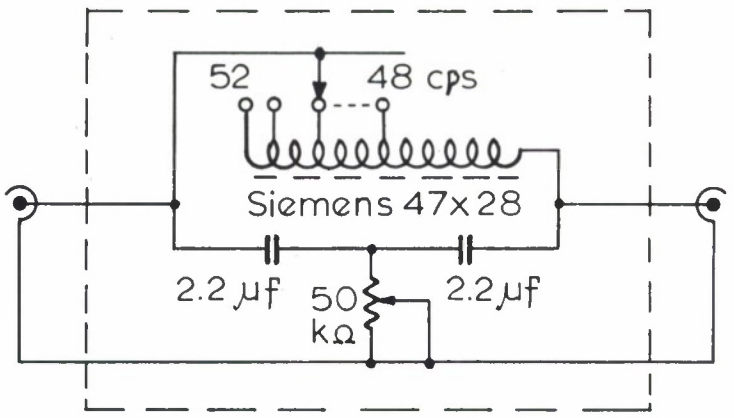

Fig. 9 Circuit diagram of the tuneable Power-Line Filter.

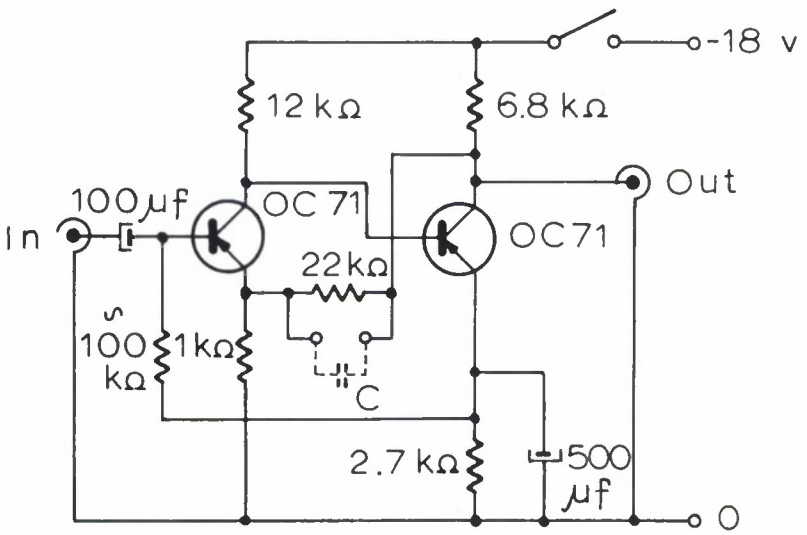

Fig. 10 Circuit diagram of one section of the Main Amplifier.

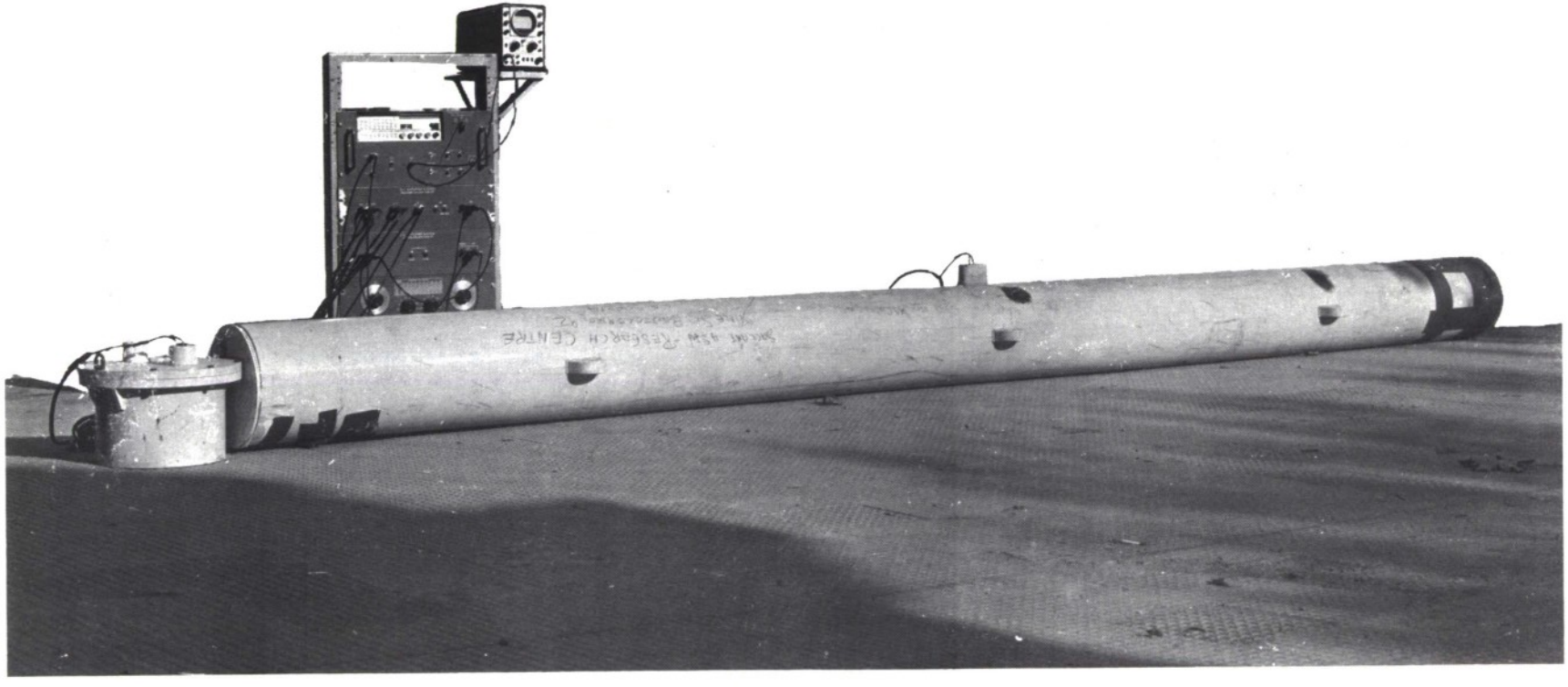

Fig. 11 An Experimental Low-Noise Electrode System, one electrode housing is shown dismounted from the tube.

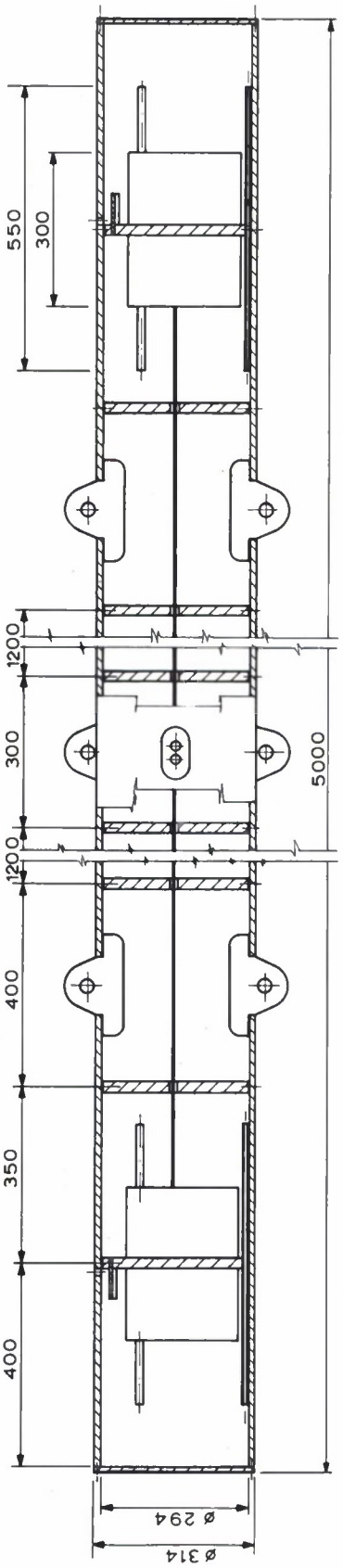

Fig. 12 Cross-section of the Electrode System.

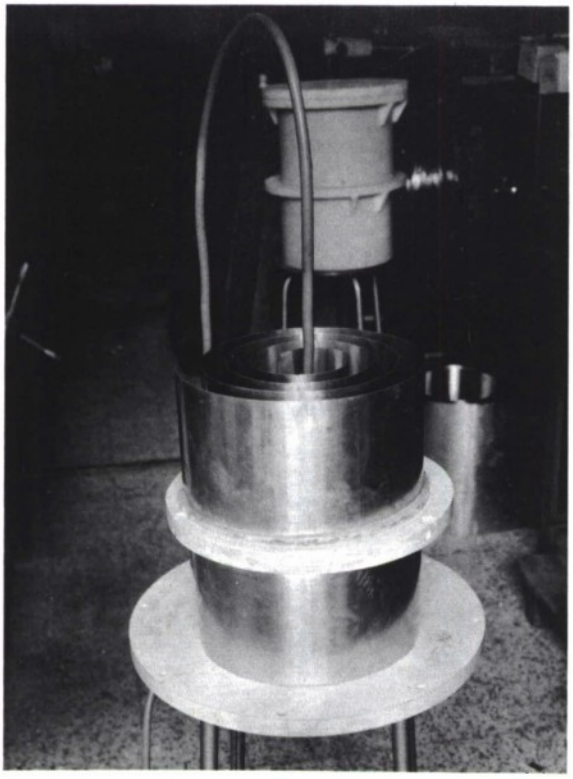

Fig. 13a. Side view of Electrode before mounting.

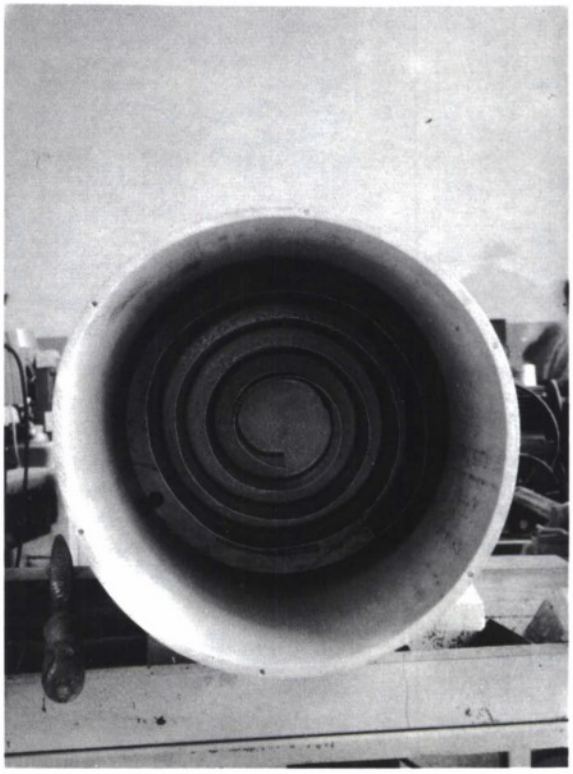

Fig. 13b. End view of Electrode mounted in the tube.

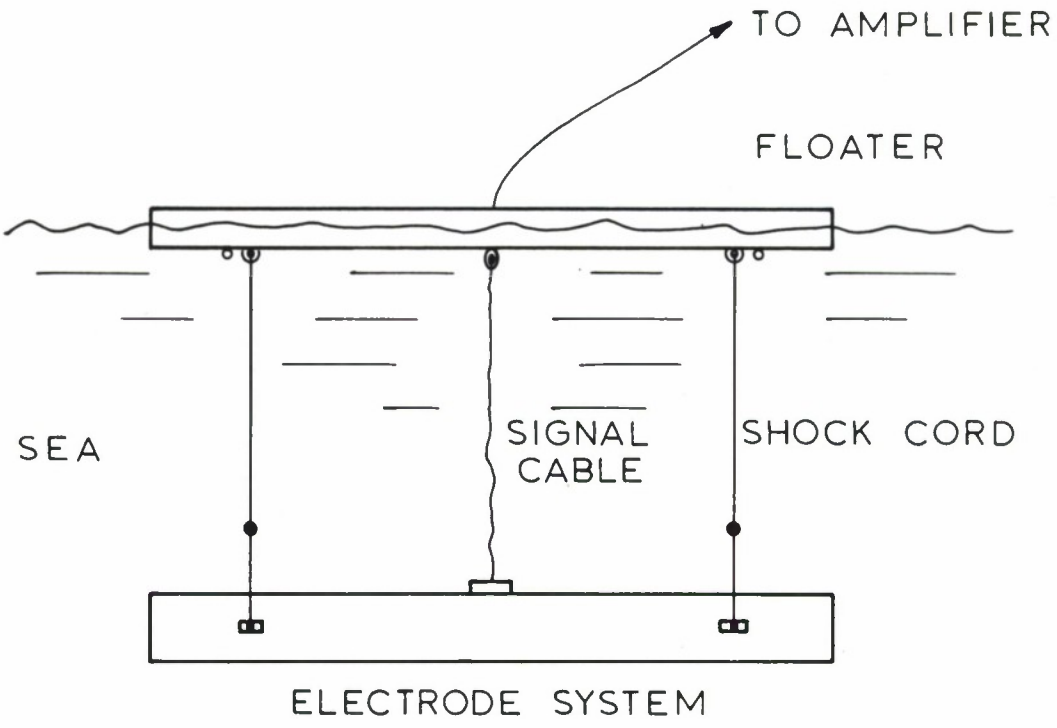

Fig. 14 Method of suspending Electrode System at sea to attenuate movement within the earth's static magnetic field.

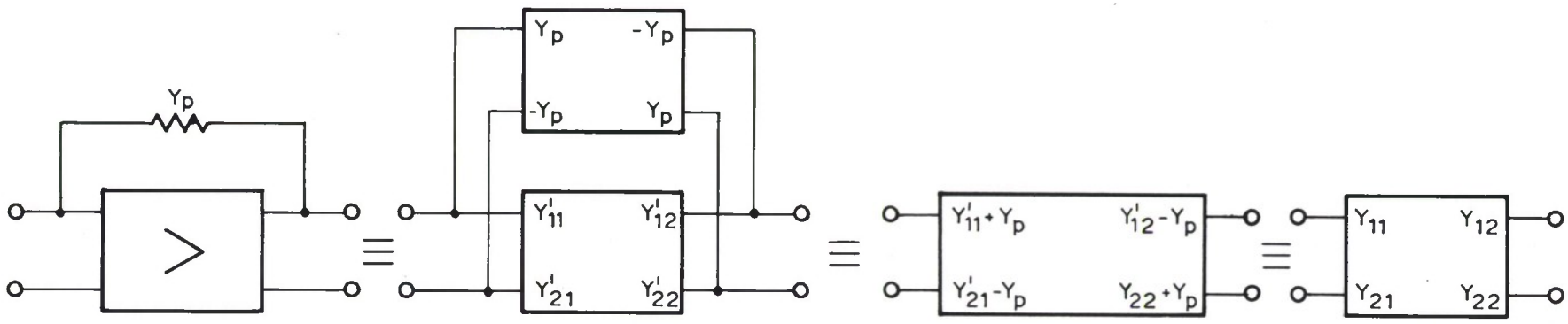

Fig. 15 Matrix representation of the Amplifier and Feedback Netowork.

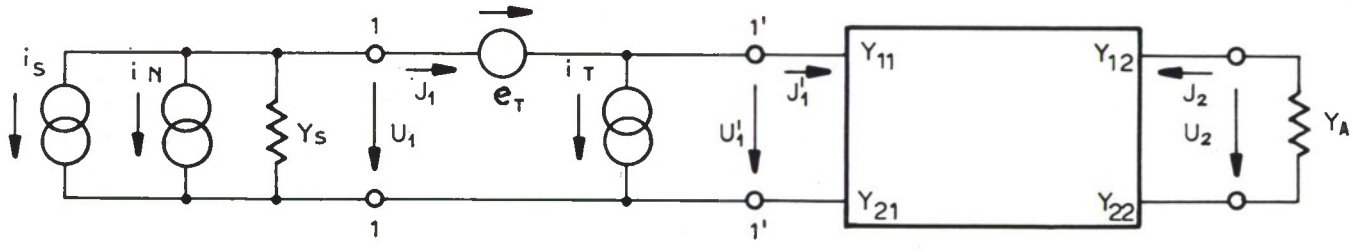

Fig. 16 Complete equivalent circuit diagram of the Amplifier and Feedback Network with all noise sources separated.

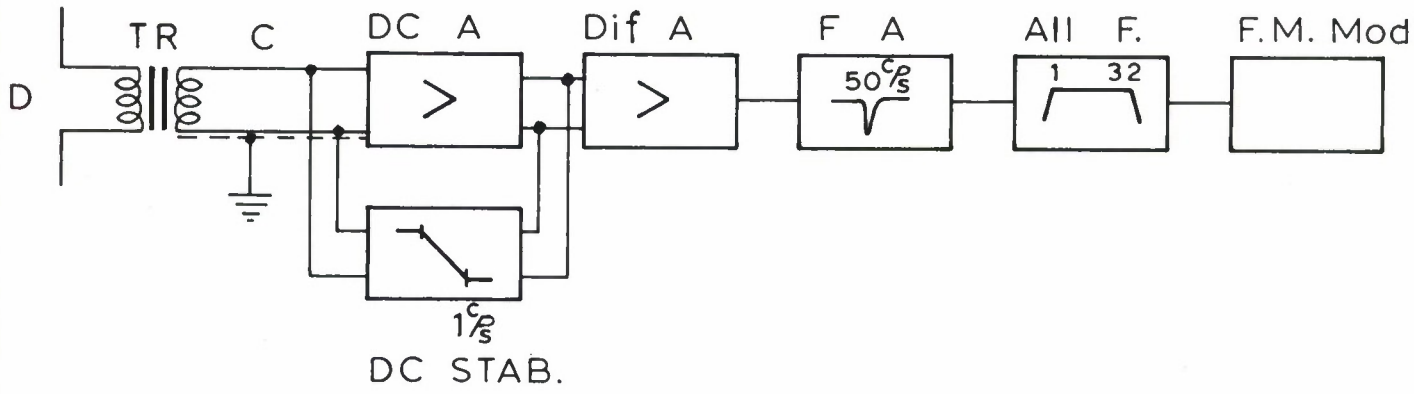

Fig. 17 Block diagram of amplifier chain.

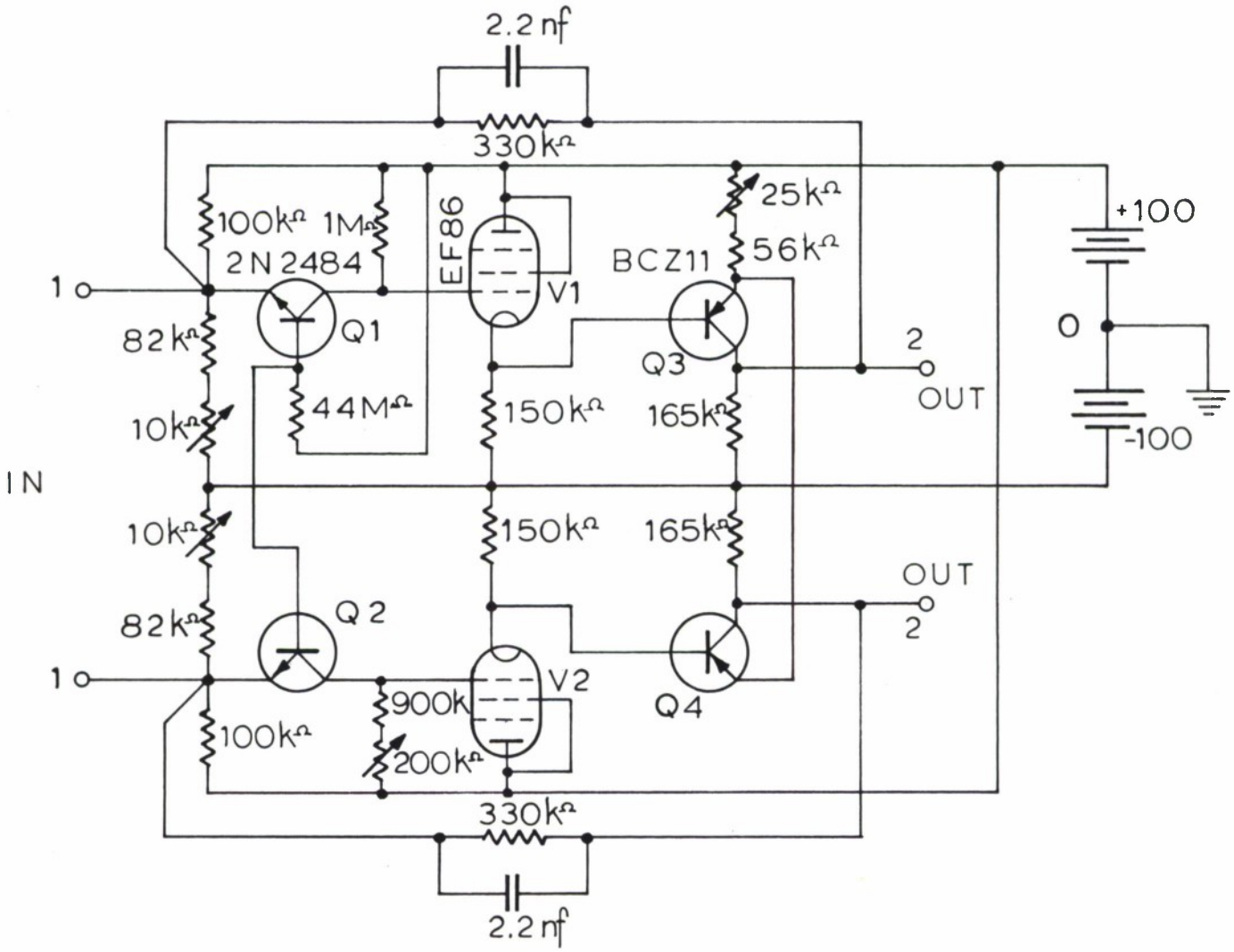

Fig. 18 Circuit diagram of DC-preamplifier.

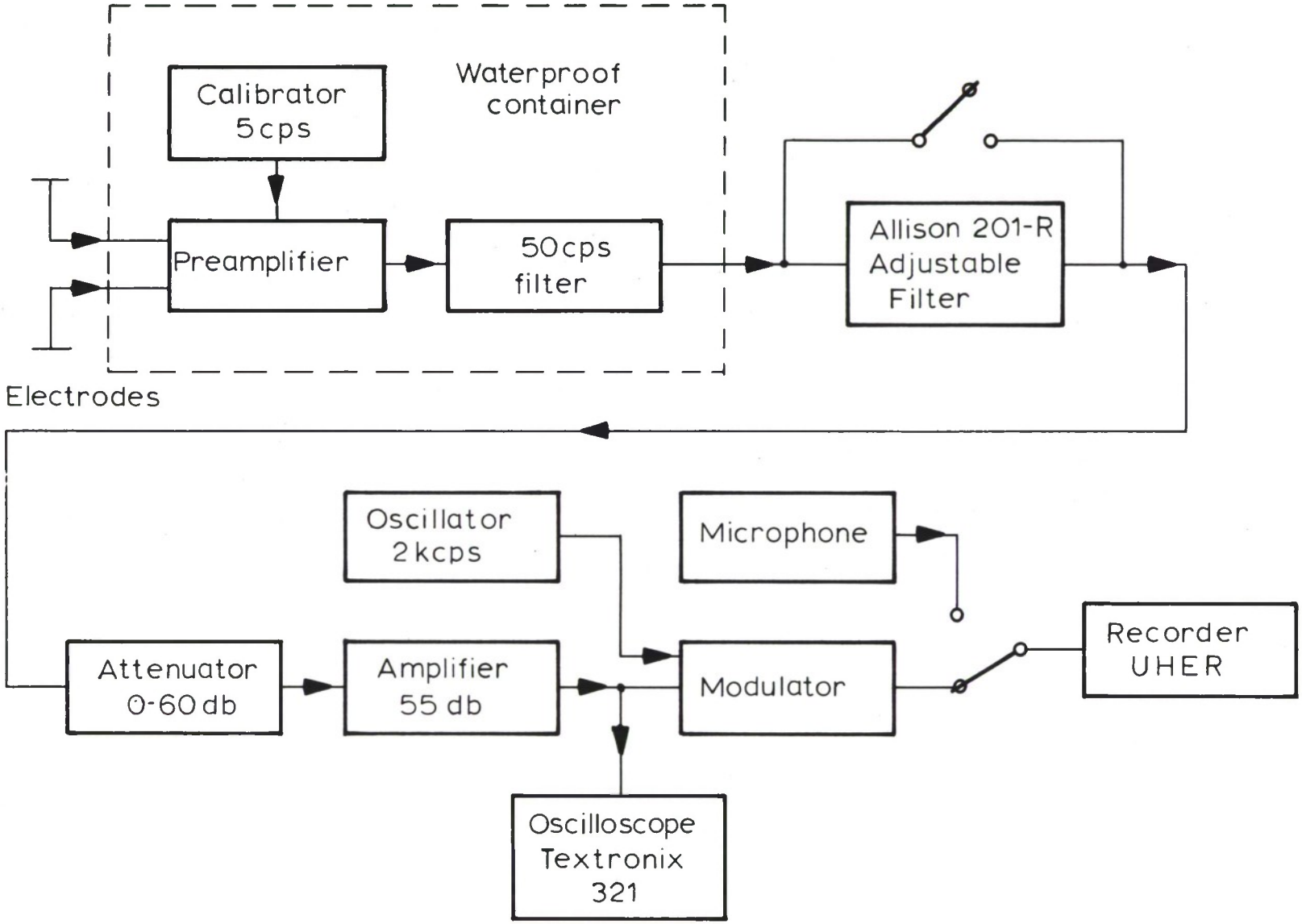

Fig. 19 Block diagram of the AM Modulator.

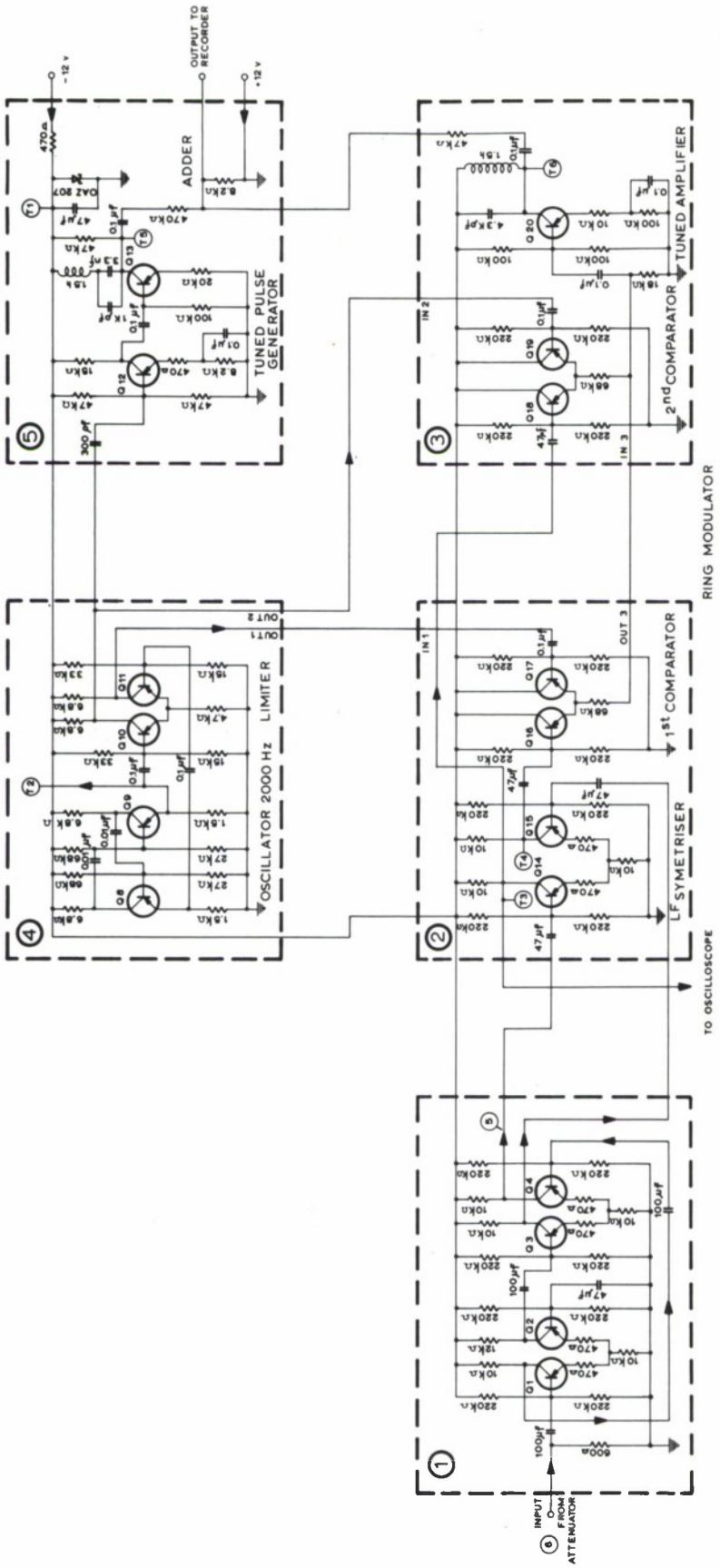

Fig. 20 Circuit diagram of the AM Modulator.

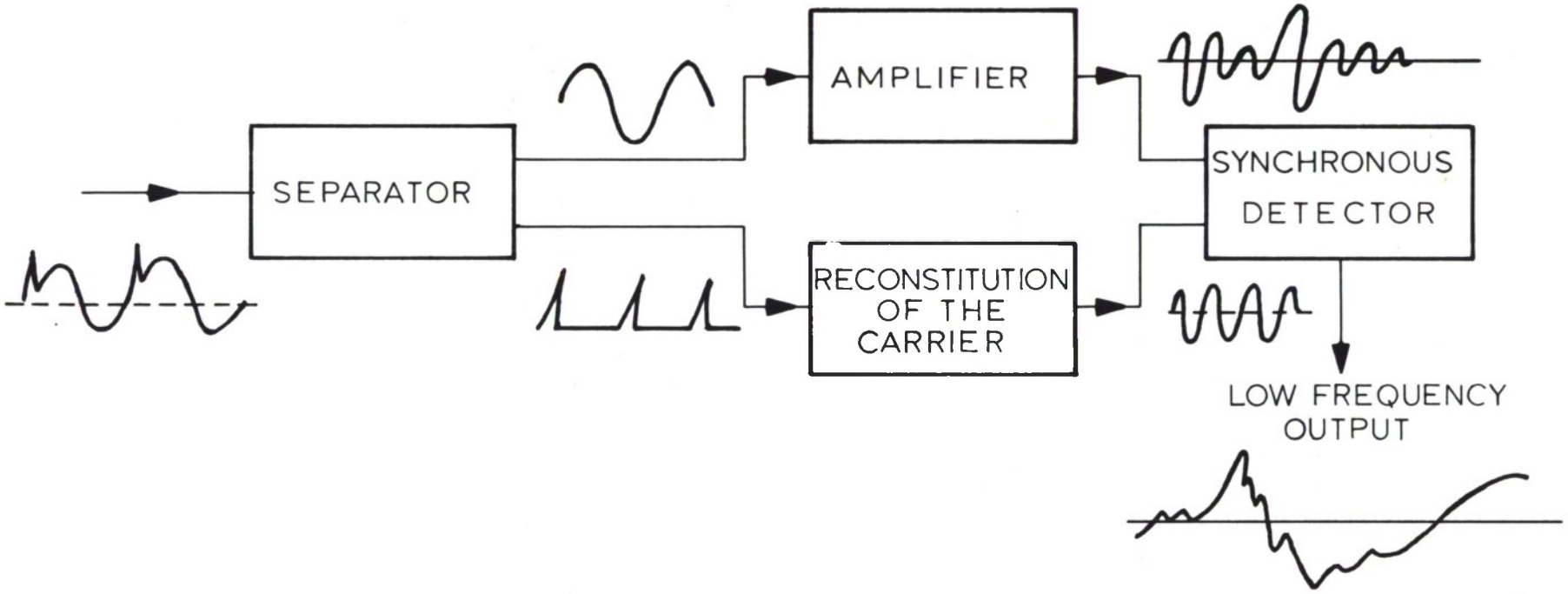

Fig. 21 Block diagram of the AM Demodulator.

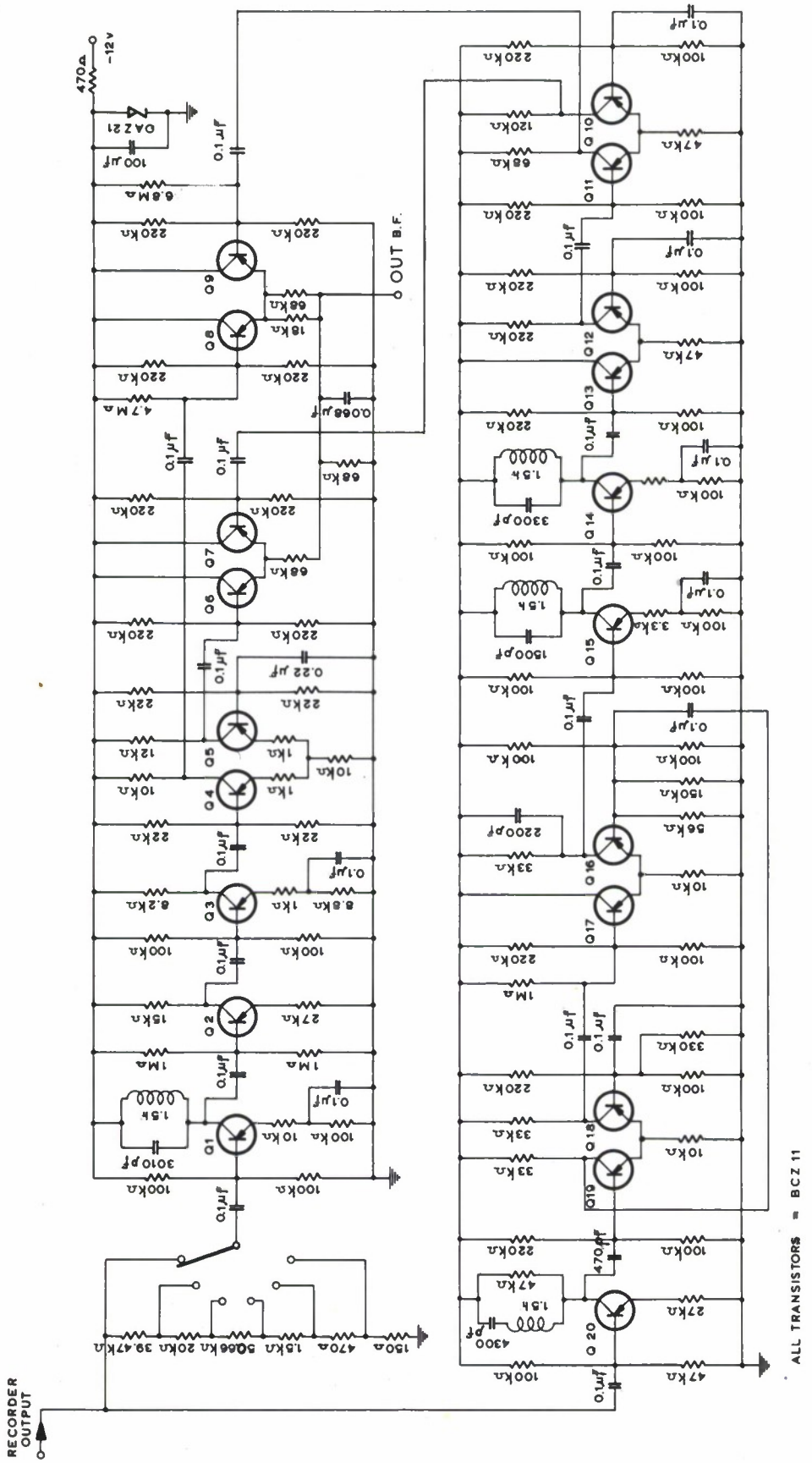

Fig. 22 Circuit diagram of the AM Demodulator.

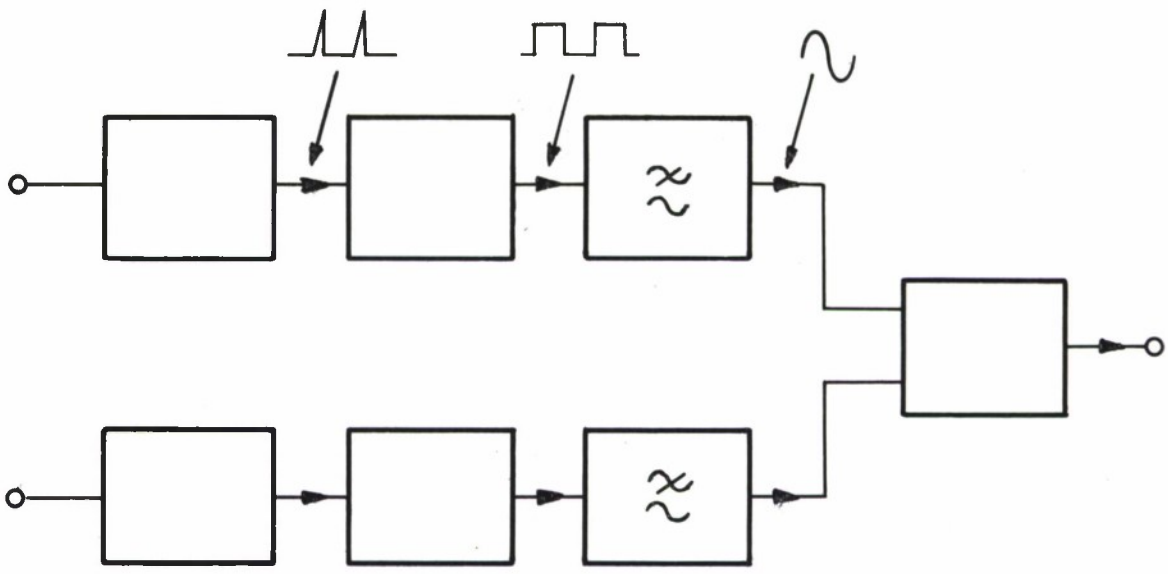

Fig. 23 Block diagram of the FM Modulator

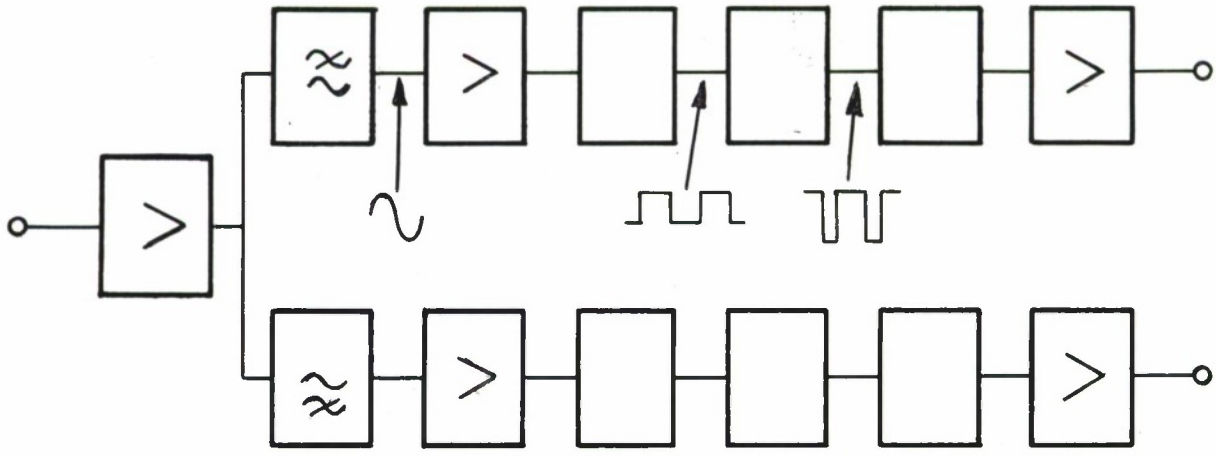

Fig. 24 Block diagram of the FM Demodulator

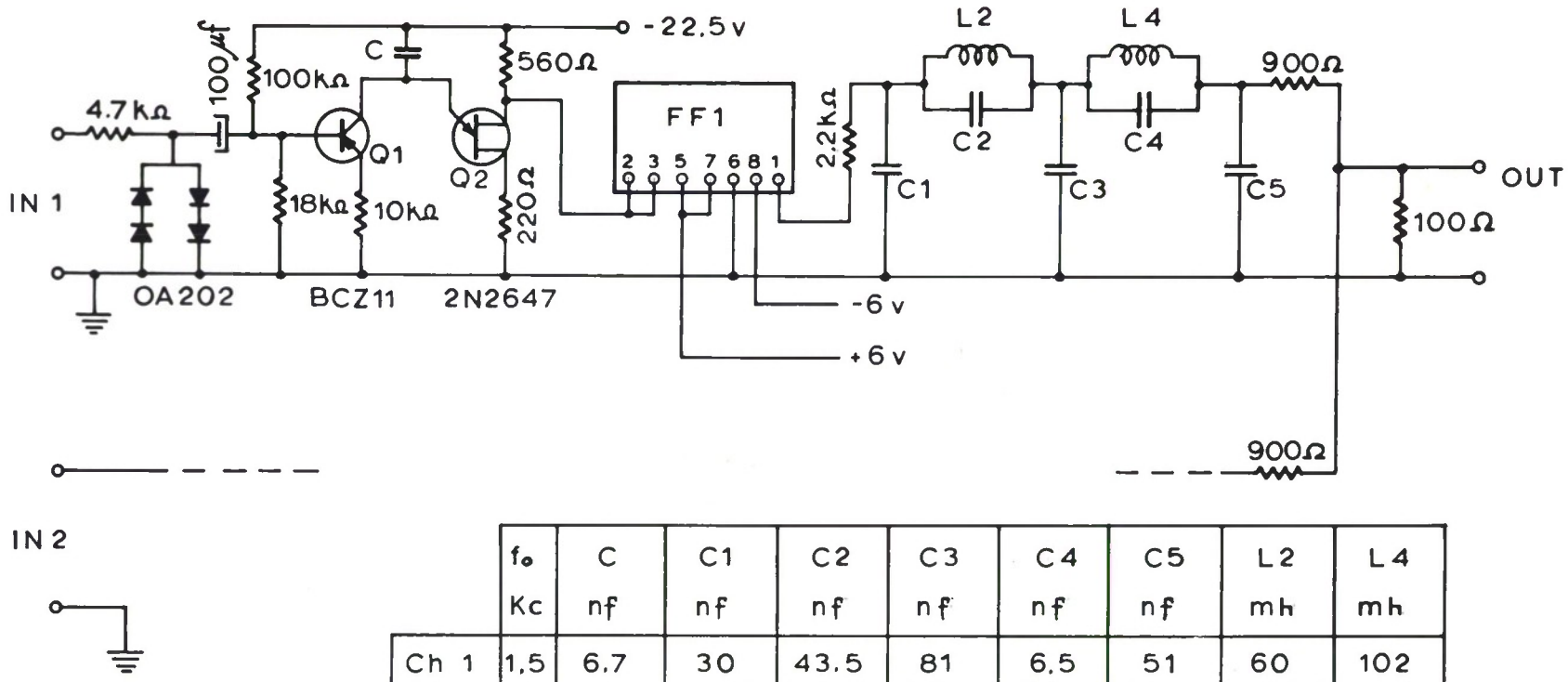

	f_o Kc	C nf	C1 nf	C2 nf	C3 nf	C4 nf	C5 nf	L2 mh	L4 mh
Ch 1	1,5	6.7	30	43.5	81	6.5	51	60	102
Ch 2	4.5	2.27	9.75	12.75	26.6	2.13	16.75	19.5	33.5

Fig. 25 Circuit diagram of the FM Demodulator.

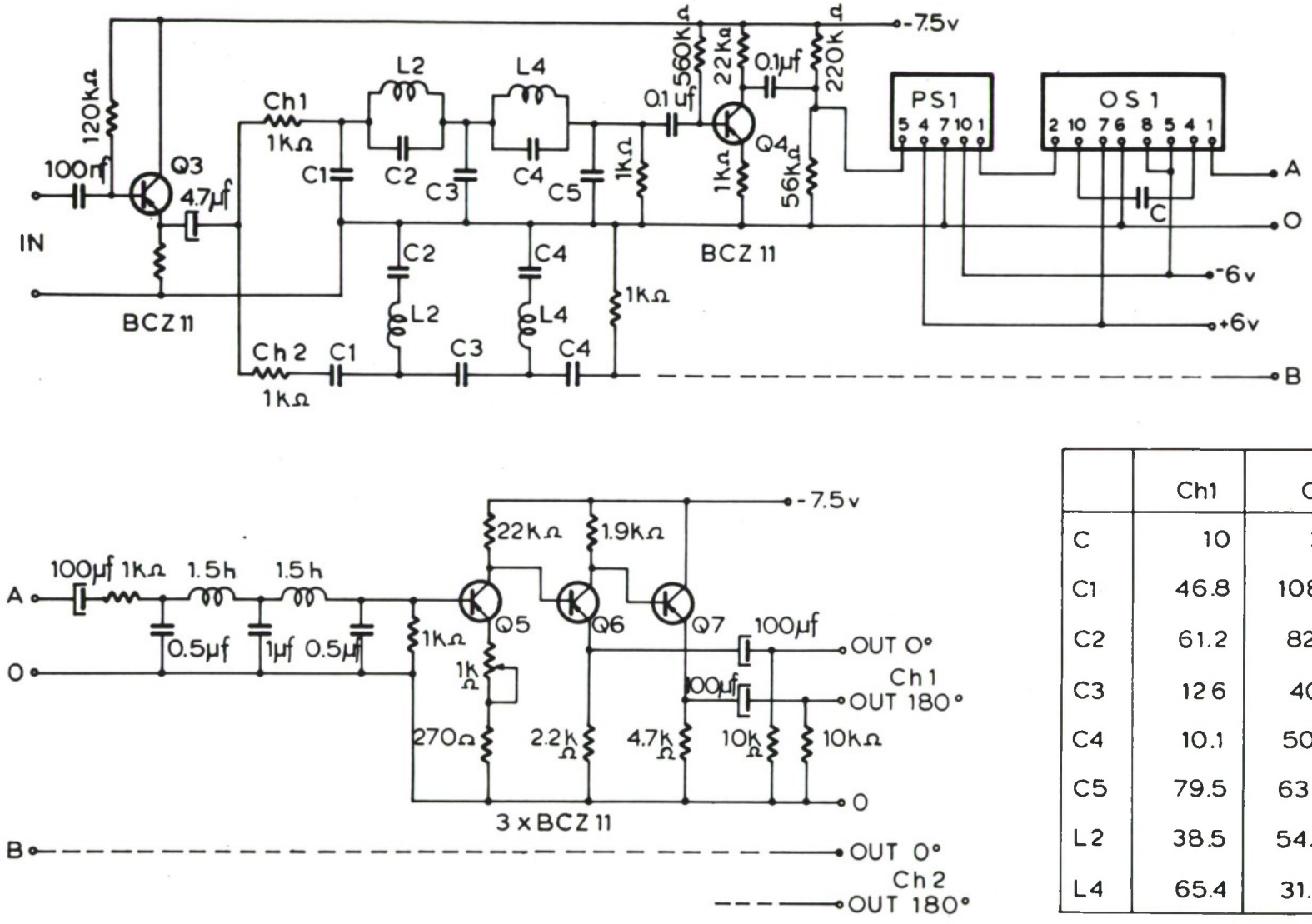

	Ch1	Ch2
C	10	3.3 nf
C1	46.8	108.4 nf
C2	61.2	82.9 nf
C3	12 6	40.1 nf
C4	10.1	500 nf
C5	79.5	63.7 nf
L2	38.5	54.2 mh
L4	65.4	31.9 mh

Fig. 26 Circuit diagram of the FM Demodulator.

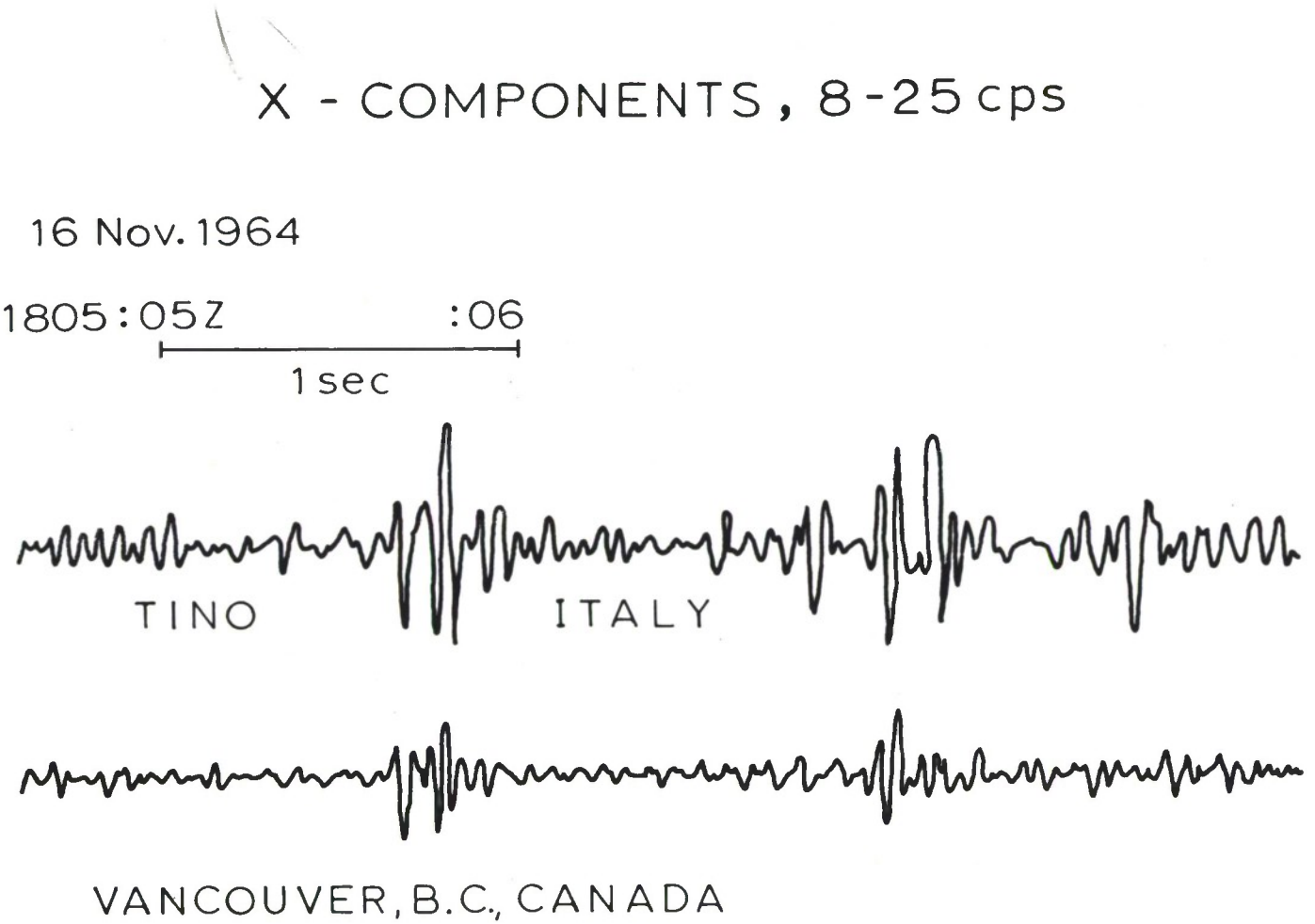

Fig. 27 Waveform Display for visual inspection — a comparison of measurements taken simultaneously in Italy and Canada.

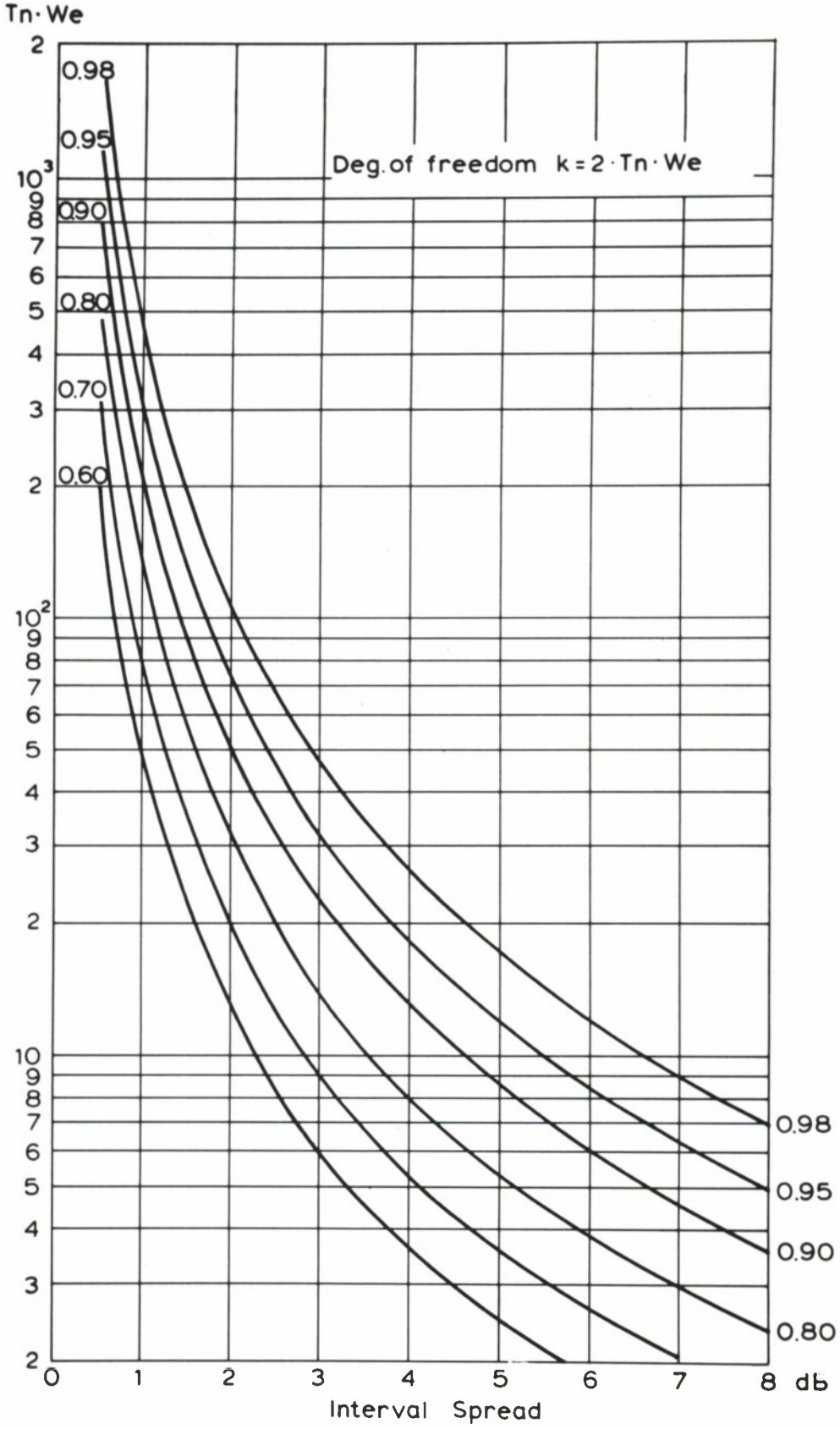

Fig. 28 Relation between the resolution, stability of measurement and sample length in power spectrum analysis, expressed in terms of degrees of freedom (vertical scale), distribution (curves) and interval spread (horizontal scale).

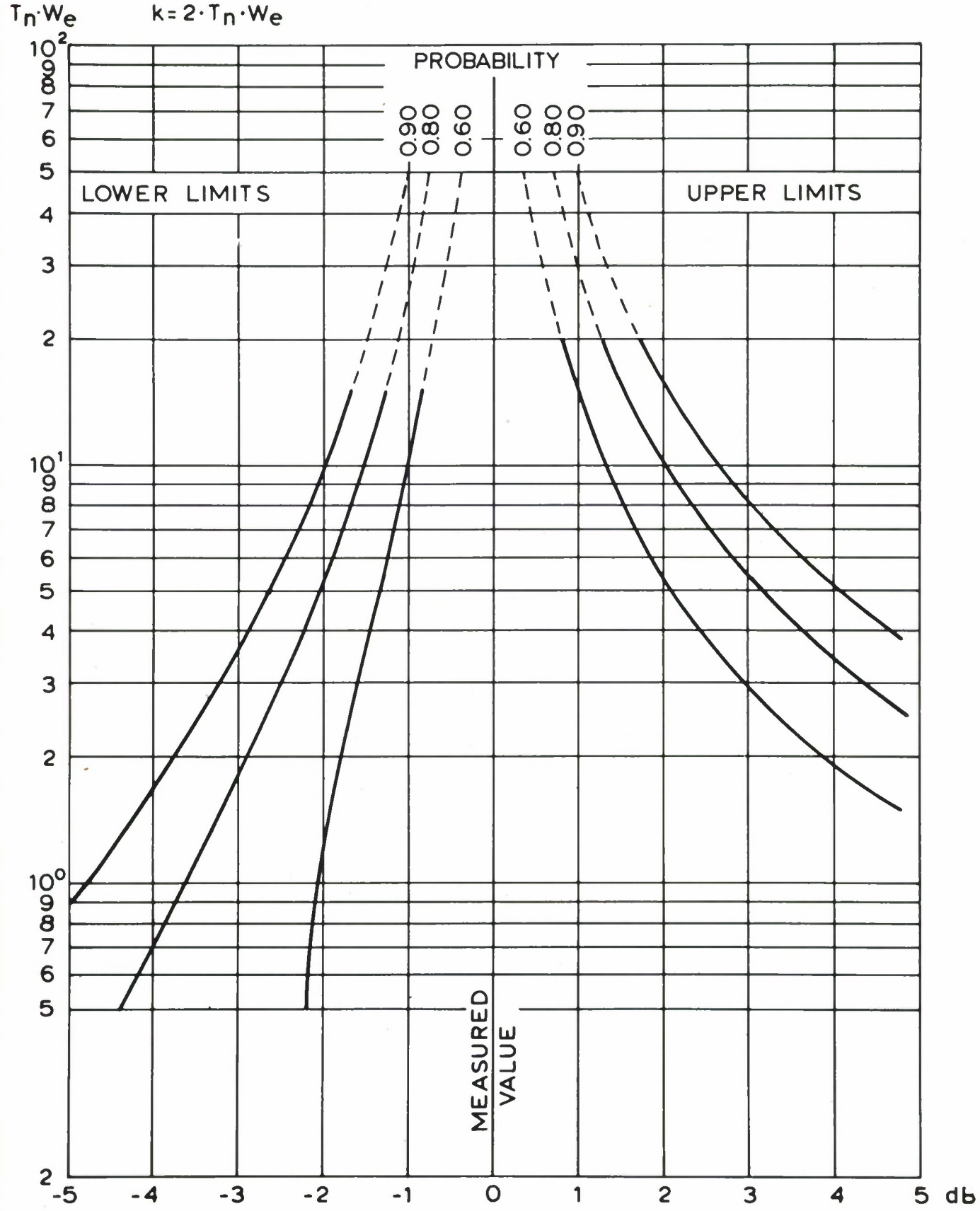

Fig. 29 Upper and lower limits to the ratio between true and measured values as a function of $T_n W_e$ and for various probabilities.

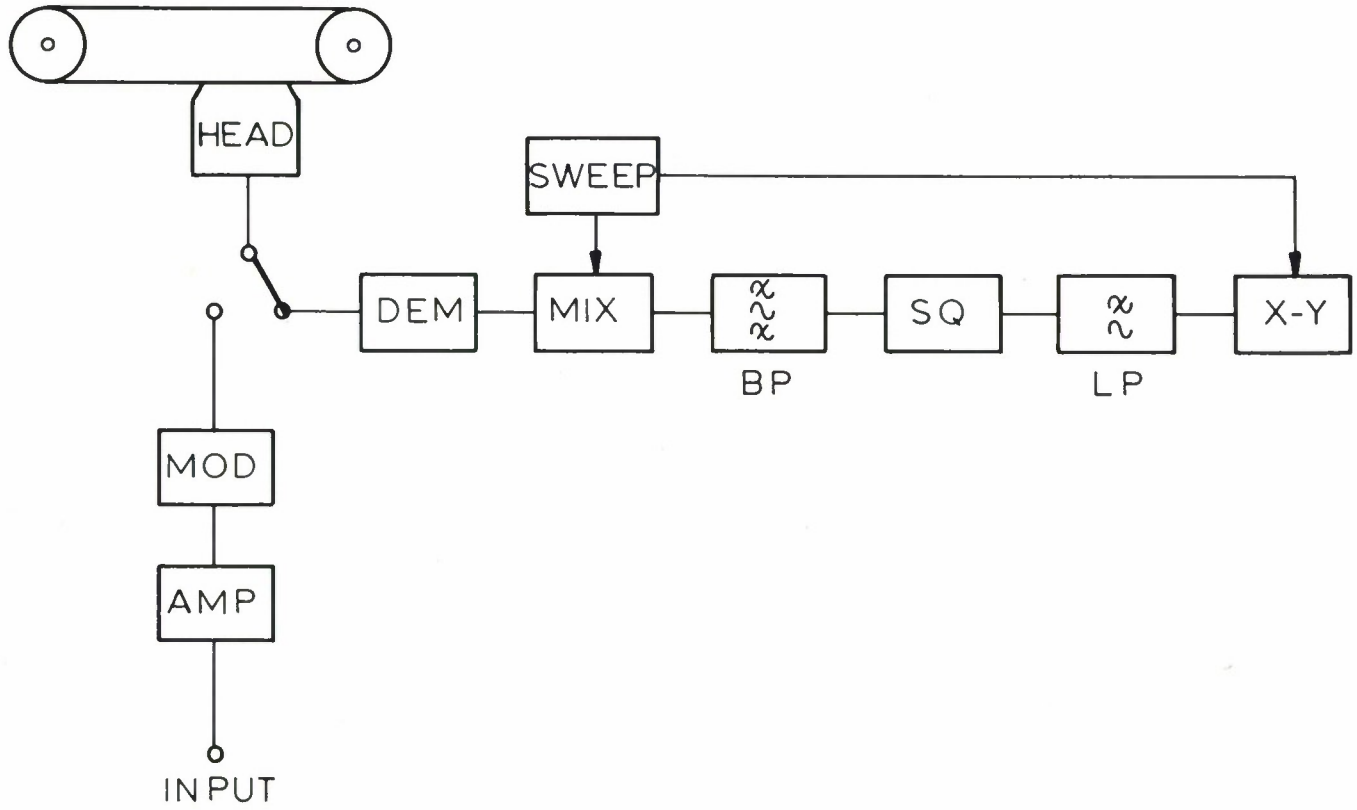

Fig. 30 Block diagram of Power Spectrum part of ISAC Computer.

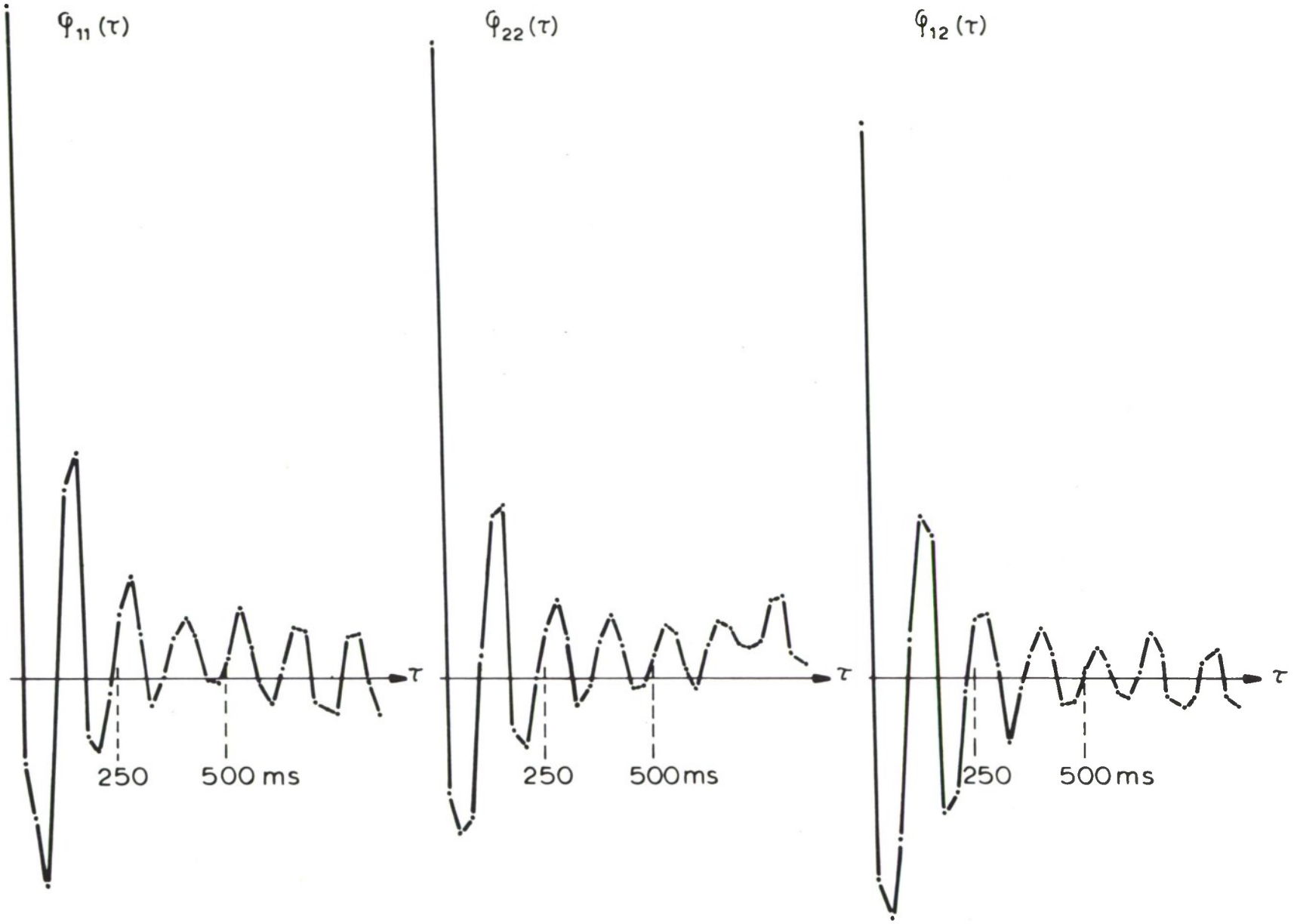

Fig. 31 Auto-correlation and cross-correlation estimates of EM background noise measured with two channels.

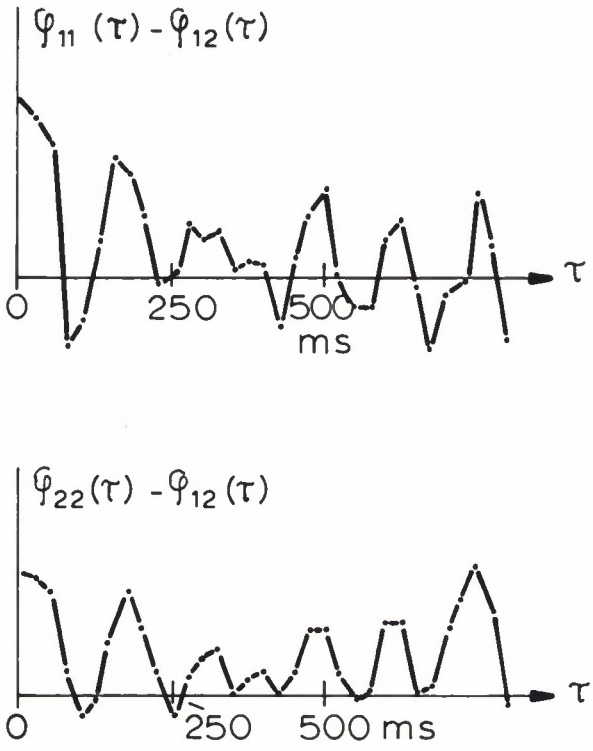

Fig. 32 Difference between the auto-correlation and cross-correlation estimates of EM background noise shown in Fig. 31.

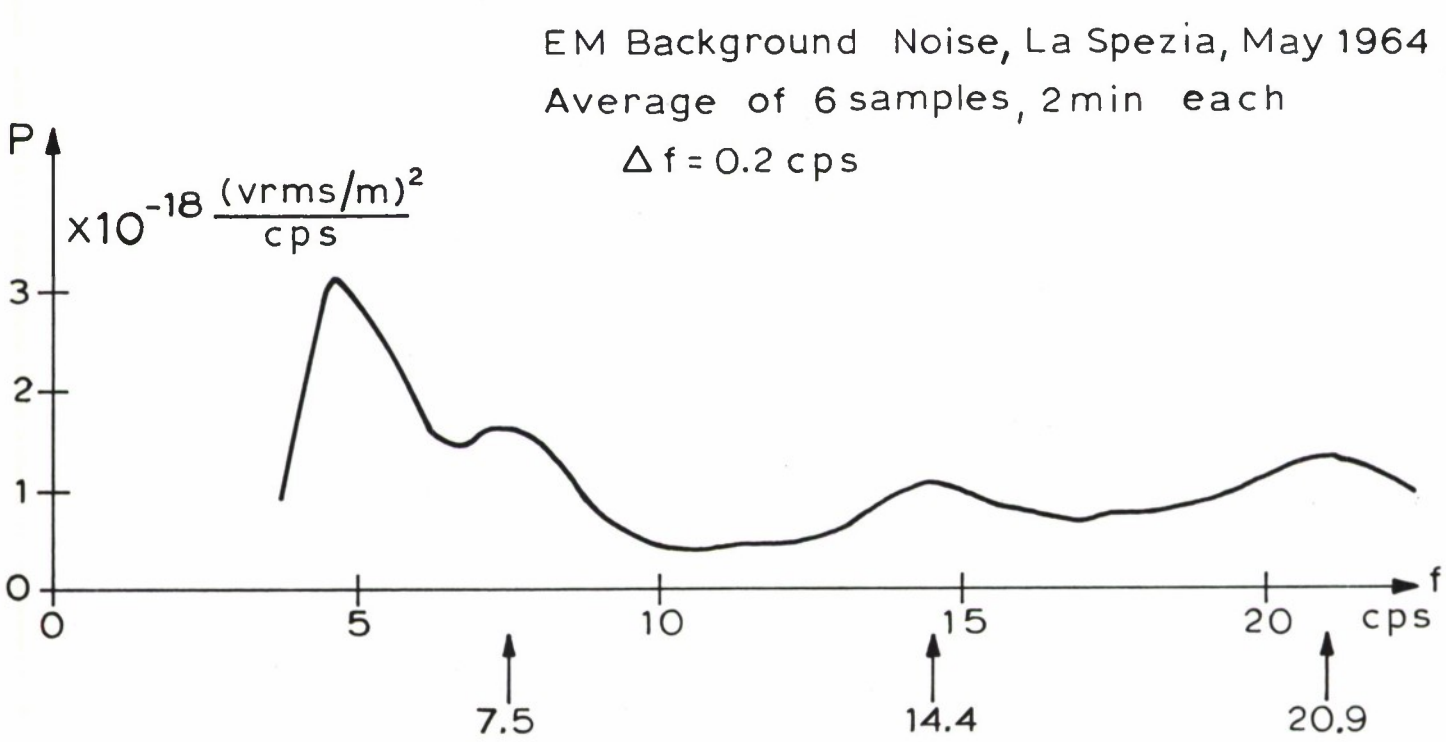

Fig. 33 Power spectrum estimate of EM background noise measured at sea in the La Spezia area.

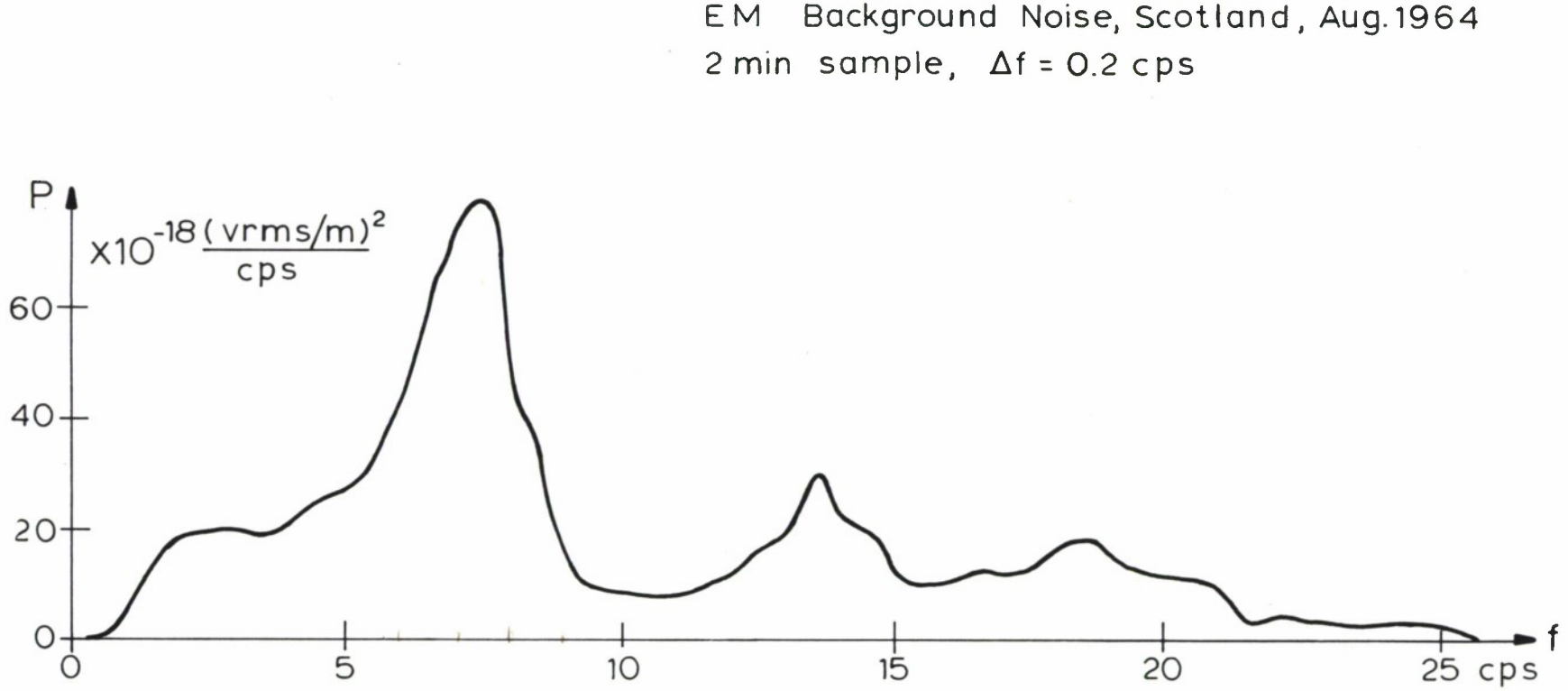

Fig. 34 Power spectrum estimate of EM background noise measured in a narrow Scottish loch.

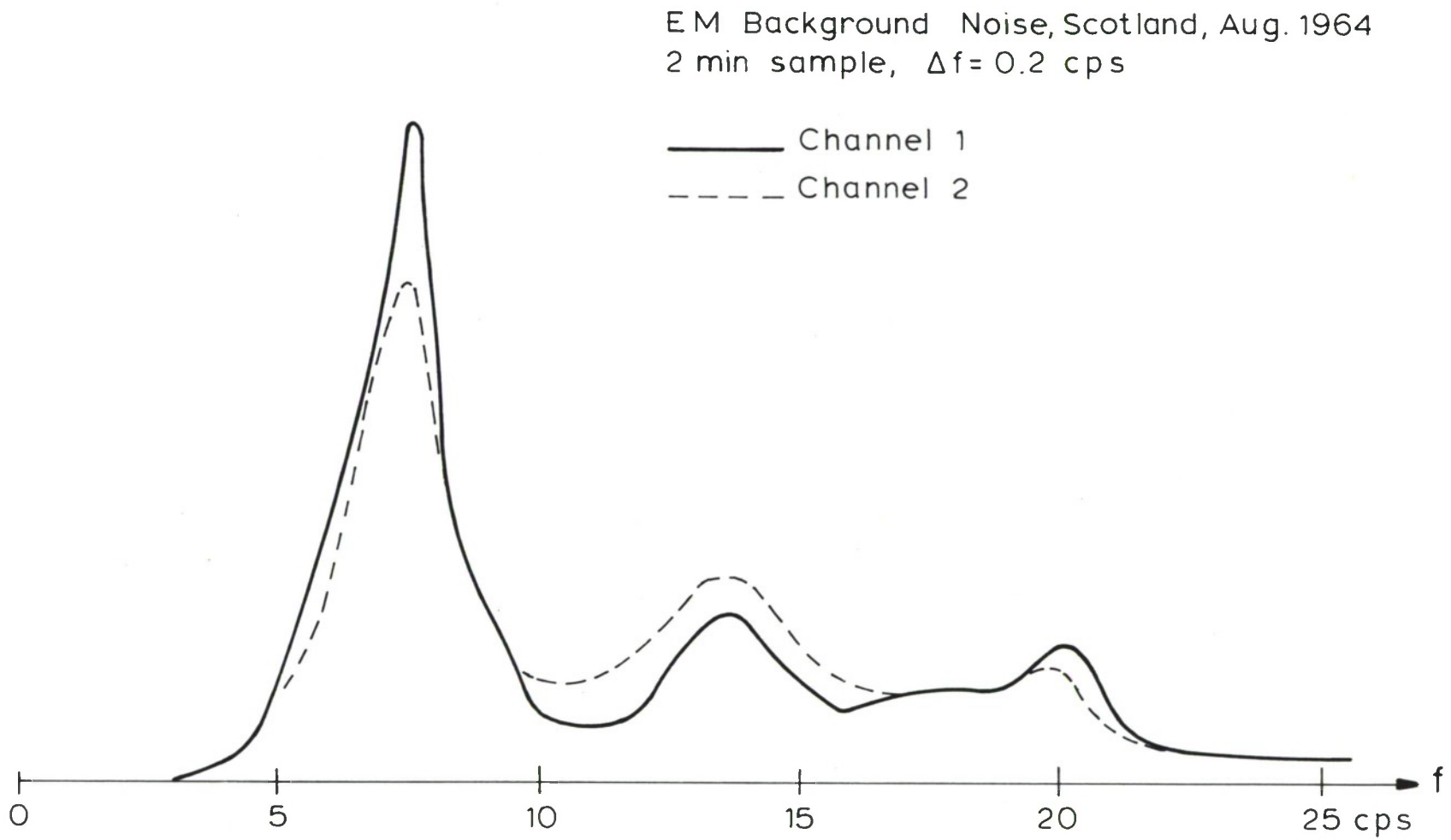

Fig. 35 Power spectrum estimate of EM background noise measured with two channels. The data are the same as for Figs. 31 and 32, with which this figure should be compared.

DISTRIBUTION LIST

Minister of Defense
Brussels, Belgium — 10 copies

Minister of National Defense
Department of National Defense
Ottawa, Canada — 10 copies

Chief of Defense, Denmark
Kastellet
Copenhagen Ø, Denmark — 10 copies

Minister of National Defense
Division Transmissione-Ecoute-Radar
51 Latour Maubourg
Paris 7e, France — 10 copies

Minister of Defense
Federal Republic of Germany
Bonn, Germany — 10 copies

Minister of Defense
Athens, Greece — 10 copies

Ministero della Difesa
Stato Maggiore Marina
Roma, Italy — 10 copies

Minister of National Defense
Plein 4, The Hague,
Netherlands — 10 copies

Minister of National Defense
Storgaten 33,
Oslo, Norway — 10 copies

Minister of National Defense
Lisboa, Portugal — 10 copies

Minister of National Defense
Ankara, Turkey — 10 copies

Minister of Defense
London, England — 20 copies

Supreme Allied Commander Atlantic
(SACLANT)
Norfolk 23511, Virginia — 3 copies

SACLANT Representative in Europe
(SACLANTREPEUR)
Place du Marechal de Lattre de Tassigny
Paris 16e, France — 1 copy

Commander in Chief
Western Atlantic Area
(CINCWESTLANT)
Norfolk 23511, Virginia — 1 copy

Commander in Chief
Eastern Atlantic Area
(CINCEASTLANT)
Eastbury Park, Northwood
Middlesex, England — 1 copy

Maritime Air Commander
Eastern Atlantic Area
(COMAIREASTLANT)
R.A.F. Northwood
Middlesex, England — 1 copy

Commander Submarine Force
Eastern Atlantic
(COMSUBEASTLANT)
Fort Blockhouse
Gosport, Hants, England — 1 copy

Commander, Canadian Atlantic
(COMCANLANT)
H.M.C. Dockyard
Halifax, Nova Scotia — 1 copy

Commander Ocean Sub-Area
(COMOCEANLANT)
Norfolk 23511, Virginia — 1 copy

Supreme Allied Commander Europe
(SACEUR)
Paris, France — 7 copies

SHAPE Technical Center
P.O. Box 174
Stadhouders Plantsoen 15
The Hague, Netherlands — 1 copy

Allied Commander in Chief Channel
(CINCCHAN)
Fort Southwick, Fareham
Hampshire, England — 1 copy

Commander Allied Maritime Air Force Channel
(COMAIRCHAN)
Northwood, England — 1 copy

Commander in Chief Allied Forces Mediterranean
(CINCAFMED)
Malta, G.C. — 1 copy

Commander South East Mediterranean
(COMEDSOUEAST)
Malta, G.C. — 1 copy

Commander Central Mediterranean
(COMEDCENT)
Naples, Italy — 1 copy

Commander Submarine Allied
Command Atlantic
(COMSUBACLANT)
Norfolk 23511, Virginia — 1 copy

Commander Submarine Mediterranean
(COMSUBMED)
Malta, G.C. — 1 copy

Standing Group, NATO
(SGN)
Room 2C256, The Pentagon
Washington 25, D.C. — 3 copies

Standing Group Representative
(SGREP)
Place du Marechal de Lattre de Tassigny
Paris 16e, France — 5 copies

ASG for Scientific Affairs
NATO
Porte Dauphine
Paris 16e, France — 1 copy

National Liaison Representatives

NLR Belgium
Belgian Military Mission
3330 Garfield Street, N.W.
Washington, D.C. — 1 copy

NLR Canada
Canadian Joint Staff
2450 Massachusetts Avenue, N.W.
Washington, D.C. — 1 copy

NLR Denmark
Danish Military Mission
3200 Massachusetts Avenue, N.W.
Washington, D.C. — 1 copy

NLR France
French Military Mission
1759 "R" Street, N.W.
Washington, D.C. — 1 copy

NLR Germany
German Military Mission
3215 Cathedral Avenue, N.W.
Washington, D.C. — 1 copy

NLR Greece
Greek Military Mission
2228 Massachusetts Avenue, N.W.
Washington, D.C. — 1 copy

NLR Italy
Italian Military Mission
3221 Garfield Street, N.W.
Washington, D.C. — 1 copy

NLR Netherlands
Netherlands Joint Staff Mission
4200 Linneau Avenue
Washington, D.C. 20008 — 1 copy

NLR Norway
Norwegian Military Mission
2720 34th Street, N.W.
Washington, D.C. — 1 copy

NLR Portugal
Portuguese Military Mission
2310 Tracy Place, N.W.
Washington, D.C. — 1 copy

NLR Turkey
Turkish Joint Staff Mission
2125 LeRoy Place, N.W.
Washington, D.C. — 1 copy

NLR United Kingdom
British Defence Staffs, Washington
3100 Massachusetts Avenue, N.W.
Washington, D.C. — 1 copy

NLR United States
SACLANT
Norfolk 23511, Virginia — 40 copies

Scientific Committee of National Representatives

Dr. W. Petrie
Defence Research Board
Department of National Defence
Ottawa, Canada — 1 copy

G. Meunier
Ingenieur en Chef des Genie Maritime
Services Technique des Constructions et
Armes Navales
8 Boulevard Victor
Paris 15e, France — 1 copy

Dr. E. Schulze
Bundesministerium der Verteidigung
ABT H ROMAN 2/3
Bonn, Germany — 1 copy

Commander A. Pettas
Ministry of National Defense
Athens, Greece — 1 copy

Professor Dr. M. Federici
Segreteria NATO
MARIPERMAN
La Spezia — 1 copy

Dr. M.W. Van Batenburg
Physisch Laboratorium RVO-TNO
Waalsdorpvlakte
The Hague, Netherlands — 1 copy

Mr. A.W. Ross
Director of Naval Physical Research
Ministry of Defence (Naval)
Bank Block
Old Admiralty Building
Whitehall, London S.W. 1 — 1 copy

Dr. J.E. Henderson
Applied Physics Laboratory
University of Washington
1013 Northeast 40th Street
Seattle 5, Washington — 1 copy

Capitaine de Fregate R.C. Lambert
Etat Major Général Force Navale
Caserne Prince Baudouin
Place Dailly
Bruxelles, Belgique — 1 copy

CAPT H. L. Prause
Sövaernets Televaesen
Lergravsvej 55
Copenhagen S', Denmark — 1 copy

Mr. F. Lied
Norwegian Defense Research
Establishment
Kjeller, Norway — 1 copy

Ing. CAPT N. Berkay
Seyir Ve HDR D
CUBUKLU
Istanbul, Turkey — 1 copy

National Liaison Officers

Mr. Sv. F. Larsen
Danish Defense Research Board
Østerbrogades Kaserne
Copenhagen Ø, Denmark — 1 copy

CDR R. J. M. Sabatier
EMM/TER
2 Rue Royale
Paris 8e, France — 1 copy

Capitano di Fregata U. Gilli
Stato Maggiore della Marina
Roma, Italia — 1 copy

LCDR J.W. Davis, USN
Office of Naval Research
Branch Office, London
Box 39, Fleet Post Office
New York, N.Y. 09510 — 1 copy

CDR Jose E.E.C. de Ataide
Instituto Hydrografico
Rua Do Arsenal Porta H-1
Lisboa 2, Portugal — 1 copy